EVALUATION OF A DUAL-MODE, TURBOJET-TURBOPROP ENGINE FOR UNMANNED AIRCRAFT

By

TREY SCHINZLER

Bachelor of Science in Aerospace Engineering

Oklahoma State University

Stillwater, OK

2020

Bachelor of Science in Mechanical Engineering

Oklahoma State University

Stillwater, OK

2020

Submitted to the Faculty of the
Graduate College of the
Oklahoma State University
in partial fulfillment of
the requirements for
the Degree of
MASTER OF SCIENCE OR ARTS
May, 2022

EVALUATION OF A DUAL-MODE, TURBOJET-TURBOPROP ENGINE FOR UNMANNED AIRCRAFT

Thesis Approved:

Dr. Kurt Rouser

Thesis Adviser

Dr. Rick Gaeta

Dr. Jamey Jacob

ACKNOWLEDGEMENTS

The author would like to thank Dr. Kurt Rouser for assistance in the direction of this study. The author would also like to thank research assistants Seth Robbins, Joey Vita, Zach Wattenbarger, James Masoner, Johnathan Burgess for assistance in engine analysis and tests.

Name: TREY SCHINZLER

Date of Degree: MAY, 2022

Title of Study: EVALUATION OF A DUAL-MODE, TURBOJET-TURBOPROP ENGINE FOR UNMANNED AIRCRAFT

Major Field: MECHANICAL AND AEROSPACE ENGINEERING

Abstract: This paper provides experimental feedback on the feasibility of a small-scale, dual-mode turbojet to turboprop engine. The engine used for testing was a KingTech K45-TP. Key parameters focused on for this experiment were turbojet and turboprop thrust. A parametric cycle analysis was performed on a pure turbojet configuration and turboprop configuration, then using mass flow parameter various nozzles were sized to be designed and tested. Mission analysis was also performed to get an idea of the required thrust that could be expected for takeoff and flight. The experiment examines the effect of turbojet thrust with respect to varying nozzle exit diameters, as well as nozzle location relative to the exhaust exit. The engine was run in both turbojet mode and turboprop mode with the various nozzle designs with exit diameters measuring from roughly 1.5 inches to 1 inch. During each test, the nozzles started at a backoff distance of two inches and as the engine was running the nozzles were moved forward at quarter inch increments until the backoff distance was half an inch. While running the engine in turbojet mode, there was a highlighted focus on a potential performance increase in turbojet thrust as the nozzles were moved closer to the exhaust. While running the engine in turboprop mode, the highlighted focus was if there was a performance decrease in turboprop thrust as the nozzles were moved closer to the exhaust. Results show that there is an optimal nozzle geometry and placement for turbojet mode, with little effect while running in turboprop mode. Overall, the turbojet thrust recorded during testing is found to be inadequate for high-speed cruise, however the thrust that is produced could be useful for a transition to turboprop mode from a RATO takeoff with a propeller lock.

TABLE OF CONTENTS

LIST OF TABLES

Table Page

LIST OF FIGURES

Figure Page

Figure Page

NOMENCLATURE

AR	aspect ratio
α	ratio of primary to secondary flow inlet areas
β	propeller pitch angle, deg
C_C	core output coefficient
C_D	drag coefficient
C_L	lift coefficient
C_{prop}	propeller output coefficient
C_{tot}	total output coefficient
c_{pc}	specific heat before combustion, BTU/lbm*R
c_{pt}	specific heat after combustion, BTU/lbm*R
d	diameter, in
D	drag, lb
E	aircraft endurance, min
F	thrust, lb
f	acceleration due to gravity, m/s^2
gc	gravitational proportionality constant, lbm*ft/lbf*s^2
GSU	ground support unit
γ	ratio of specific heat

h_{PR}	heat capacity of fuel, BTU/lbm
η	efficiency
LOT	Level of Technology
M	Mach number
MFP	Mass Flow Parameter
$\dot{m}$	mass flow rate, lbm/s
p	blade pitch, in
P	pressure, psi
PCA	Parametric Cycle Analysis
Φ	installation losses
r	radius, in
ρ	density, lbm/ft^3
π	pressure ratio
RPM	rotations per minute
s	sample standard deviation
S	wing area, ft^2
SFC	Specific Fuel Consumption
SPL	Sound Pressure Level, dB
sUAS	Small Unmanned Aircraft Systems
T	temperature, °F
TP	turboprop
TSFC	Thrust Specific Fuel Consumption
θ	measurement angle, deg

U	velocity, ft/s
UAS	Unmanned Aircraft Systems
UDF	Unducted Fan
V	velocity, ft/s
VC	Variable-Cycle
Wt	aircraft weight, lb

Subscripts

avg	average
b	combustor, burner
c	compressor
d	diffuser
f	fuel
j	jet
mech	mechanical shaft
prop	propeller
t	total or stagnation property
0	ambient, freestream
2	compressor inlet
3	combustor inlet
4	turbine inlet
5	turbine exit
9	nozzle exit

CHAPTER I

INTRODUCTION

1.1.1 Problem

Small, unmanned aircraft (Group I or II) typically desire two performance capabilities, high-speed flight, and good fuel economy. Table 1 shows the specifications for group I and II UAS. The problem, however, is a tradeoff between the two. A turbojet is a design choice for high-speed flight bur has poor thrust specific fuel consumption (TSFC). TSFC is the rate of fuel used by the propulsion system per unit thrust produced. A turboprop achieves a better (lower) TSFC than a turbojet but will typically not fly as fast. Figure 1 shows the characteristics of TSFC for typical aircraft engines. The challenge is to achieve a compromise between the two performance parameters with the same engine. This problem has two potential solutions; first, develop an in-between engine specifically for UAS or develop an engine capable of switching between the two different propulsion cycles to better optimize performance. A variable cycle engine enables us to achieve both.

Table 1: UAS Group I and II Specifications

UAS Category	Max GTOW (lbf)	Normal Operating Altitude (ft)	Speed (KIAS)	Representative UAS
I	1-20	< 1200 AGL	100	Pointer
II	21-55	<3500 AGL	< 250	ScanEagle

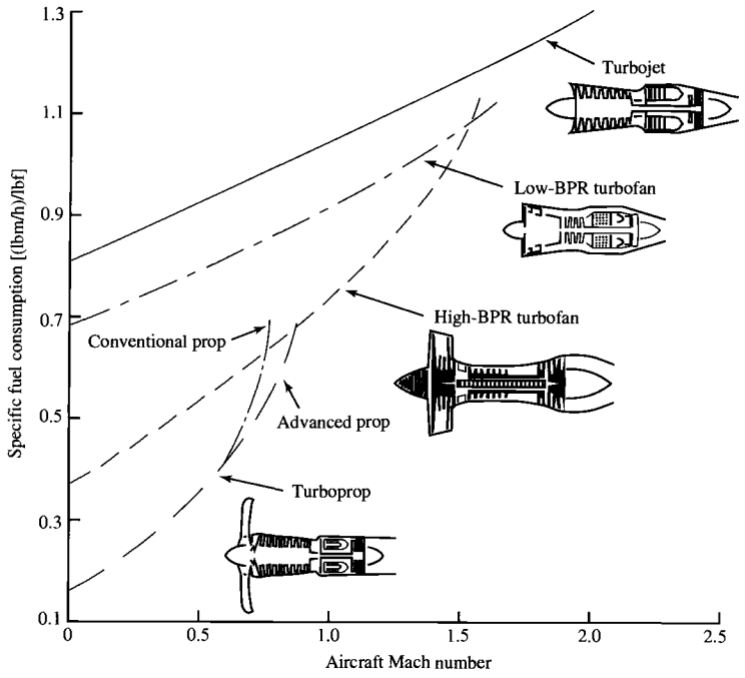

Figure 1: SFC Characteristics of Typical Aircraft Engines [5]

1.1.2 Solution

A variable cycle engine (VCE) is not a new concept. However, it has only been studied for larger engines, typically just varying bypass. The idea behind VCE is to provide optimal thrust performance or endurance at different stages of the flight envelope. VCEs function by allocating air flow through specific parts of the turbine engine. For instance, if the pilot desires more thrust,

valves, or some other method, will direct most of the air flow through the core of the engine. On the contrary, if the pilot desires better fuel economy, airflow will be directed through the bypass. The most recent VCE engine, the GE XA100, has been developed and tested, but has yet to be installed on an aircraft. VCE has yet been applied to small UAS turbine engines. The proposed solution changes the entire cycle from turbojet to turboprop. The turbojet cycle of the engine will provide the high thrust and speed desired for take-off and pursuit. Meanwhile, once the propeller engages the exhaust from the turbojet, the power can be throttled back for optimal endurance and efficiency for loiter and cruise. The main challenge with this current solution is developing viable turbojet thrust.

Figure 2: KingTech K45-TP [6]

1.1.3 Objective

In this current study a 7 hp (52 kW) KingTech K45-TP turboprop is used. Methods are created to test the engine as a pure turbojet and a turboprop. Experiments examine the effect of turbojet thrust with respect to nozzle geometry, as well as nozzle location relative to the turboprop exhaust exit. In addition to turbojet thrust, the effect of turboprop thrust is also evaluated running the same experiments with the varying nozzle geometries at different backoff distances. The

purpose behind these experiments is to determine if viable turbojet thrust can be produced by the engine, as well determining if nozzles at a certain distance have any significant impact on the turboprop. A variety of different propellers are used to evaluate the effectiveness of turboprop thrust, specifically fixed propeller blades versus folding propeller blades. Experiments in the OSU sub-sonic wind tunnel evaluate thrust coefficient and propeller efficiency, tested over a range of airspeeds and RPMs. This experiment sets up the potential for multiple future projects.

CHAPTER II

BACKGROUND

2.1 Gas Turbine Engines

Gas turbine engines include an inlet, compressor, combustor, turbine, and a nozzle. The turbine on the engine extracts air from the core flow after fuel has been mixed and combustion has occurred. The turbine is attached to the compressor by shaft. A turbojet cycle is composed of the five engine stages as mentions above: inlet, compressor, combustor, turbine, nozzle, and sometimes an afterburner. Engine cycles vary based on additional engine components. For instance, a turboprop engine is very similar to a turbojet engine. However, a turboprop has an additional turbine, aft of the core turbine, that drives a propeller. In the figure below a distinction is made between the two with simplified schematics.

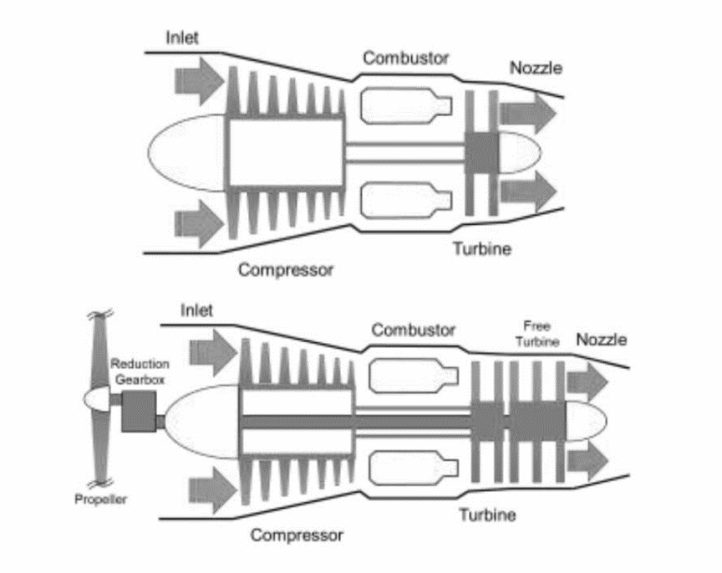

Figure 3: Turbojet Schematic (top), Turboprop Schematic (bottom) [5]

Turbojet engines are usually used for high-speed applications due to having high speed exhaust, but they also have a higher thrust specific fuel consumption. Thrust specific fuel consumption is the mass flow rate of fuel for every unit of thrust produced. Turboprops, despite being like a turbojet, is the exact opposite relative to these to parameters. A turboprop has a much lower thrust specific fuel consumption but is constrained to lower speeds because of the propeller. A lower thrust specific fuel consumption is achieved by distributing a large mass of air through the propeller with a slight increase in flow velocity. Figure 1 represents the thrust specific fuel consumption of both engines.

2.2 Variable Cycle Engines

The future of aircraft, whether it be commercial or military, ideally should meet certain requirements for both economic and environmental constraints. The problem is these two performance parameters are difficult to achieve with the same engine. When it comes to the design of an aircraft many compromises must be made in certain areas to fulfill the most desired

design parameter for the aircraft. The same dilemma occurs when designing engines for an aircraft. On modern aircraft, commercial and military, there are two types of engines that are commonly used, the turbojet and the turbofan. Both engines are great for what they do, however they have their tradeoffs. Turbojets are typically used for highspeed air travel. Turbofans are specifically designed for increased fuel efficiency. Turbofans have two subcategories of their own, high-bypass and low-bypass. High-bypass turbofans are optimal for fuel efficiency; however, they are not the best during takeoff since they are optimized for subsonic cruise. Low-bypass turbofans can provide supersonic capabilities but are not as efficient as the high-bypass engines. Turbofans are found on commercial aircraft for their efficient performance. An engine that could provide both performance capabilities would be more than ideal. It seems an entirely new class of engine needs to be designed to provide the best fuel efficiency when desired, while also providing more speed when desired. Variable cycle engines are the proposed solution to the dilemmas discussed over.

2.2.1 Past Variable Cycles Engine Technology

Variable cycle engines have been a propulsion concept since the 1970s. Researchers at the Lewis Research Center, in partnership with GE Aviation, Pratt & Whitney, and Boeing found that the results of trying to manufacture a VCE would be exceptionally complex [3]. They found that VCEs would be heavy and expensive to manufacture. Maintenance on such an engine would also have been something to consider; however, due to the available technology in the 70s, it seems the VCE concept was not taken too seriously. However, VCEs functionally are designed for two different modes of operation: (1) a high airflow, low jet-velocity mode for low noise takeoff and efficient subsonic cruise, and (2) a turbojet-like, higher jet-velocity, lower airflow mode for supersonic cruise [11]. Researchers at the Lewis Research Center in Cleveland, OH did a lot of

propulsion research. VCEs were included in the SCAR program (Supersonic Cruise Aircraft Research) [11]. The primary problem this research in VCE was set so solve was economical practicality. There were two methods developed to design a VCE engine. The first would rely on valves to create two or more distinct flow paths upon demand within the engine's structure [11]. The other would rely on component variability and spool speed variations [11].

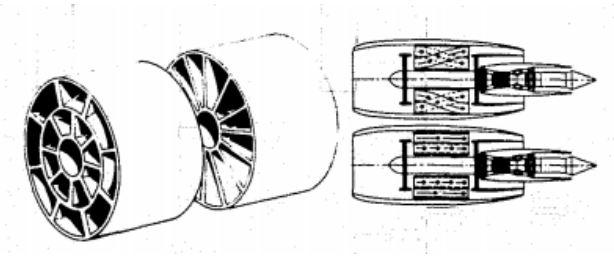

Figure 4: Early VCE Valve Concept and Series—Parallel Engine [11]

The figure above is an airflow inverting valve (AIV), which was an early concept for VCE engines. In effect, the valve can transpose the annular positions of two coaxial flow paths by indexing or rotating one-half of a cut cylinder whose facing ends mate to form the valve plane [11]. This concept would be applied to a supersonic engine between the fan and the compressor. For a "turbojet" mode the valve would be set in the straight through position, while the "turbofan" mode would be set in the crossover position seen in Figure 4 [11]. However, after further examination this design was found to be heavily flawed, due to pressure loss penalties and added weight [11]. With more iterations of the valve designs methods were made that provided very attractive performance in both takeoff and cruise, however the added weight of the valves countered any performance gains. For this problem, a new challenge was to make lighter engines overall. Then Pratt & Whitney invented the inverted throttle schedule, or ITS [11]. This

technique allowed engine to maintain an optimal inlet match for the entire subsonic to supersonic flight regime [11]. This method provided great SFC improvements.

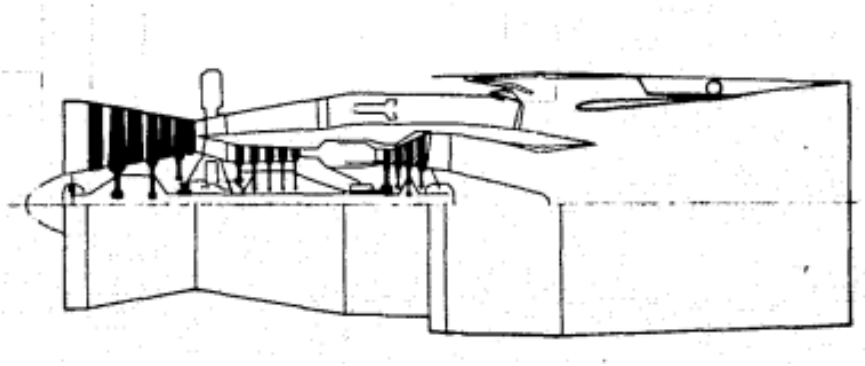

Figure 5: Variable Steam Control Engine [11]

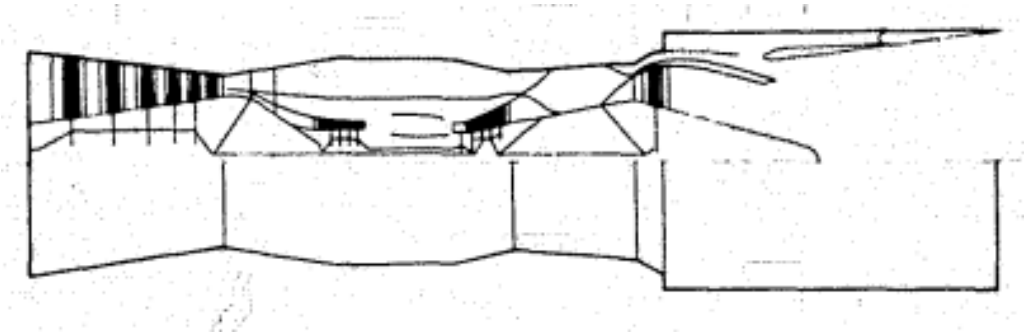

Figure 6: Rear Valve Variable Cycle Engine [11]

The engines seen in Figures 4 and 5 are the final the two engine designs after further refinement and technology advancement implications. The engine in Figure 5, the variable steam control engine (VSCE), has a flow path of a conventional duct heated turbofan and incorporates ITS with a variable geometry fan [11]. This engine was able to perform well under both desired operating modes. The engine in Figure 6, the rear valve variable cycle engine (RVVCE), this design is more in line with the changing flow path approach to the VCE solution. The crossover position of the valve provides optimal performance of that of a supersonic engine, while

eliminating the losses that were resulting in prior designs. Meanwhile the pass-through position provided optimized performance for subsonic cruise, while also eliminating losses found in earlier designs.

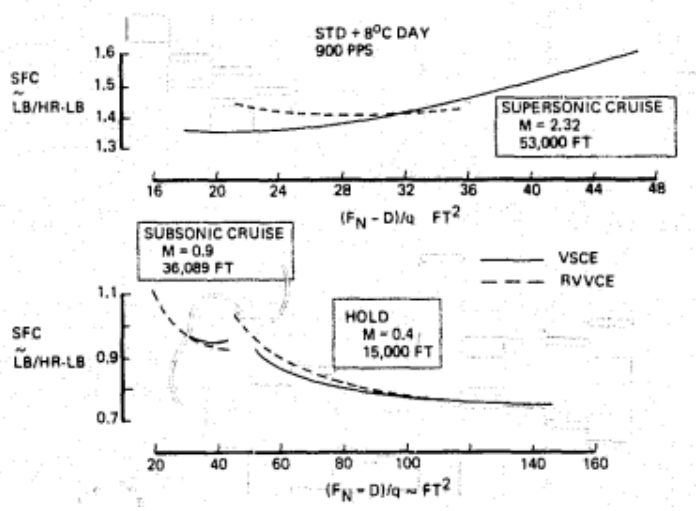

Figure 7: Engine Installed Performance Comparison [11]

With modern technology commercial air travel has become more practical without the primary benefits of using a VCE. At the end of this research a list of requirements for VCE engines was developed. The list included: co-annular nozzles, clean-efficient duct burner, variable geometry fans, hot section technology, inlets, electronic controls, and airplane/engine integration [11]. However, potential customers are still skeptical of the technology available to produce such an engine and if that endeavor is practical. While VCEs where an impractical alternative for supersonic cruise in the 70s, they were a substantially attractive method for hypersonic travel. Pratt & Whitney was able to develop the J58, which was used to power the SR-71 Blackbird, capable of traveling at speed greater than Mach 3 [5].

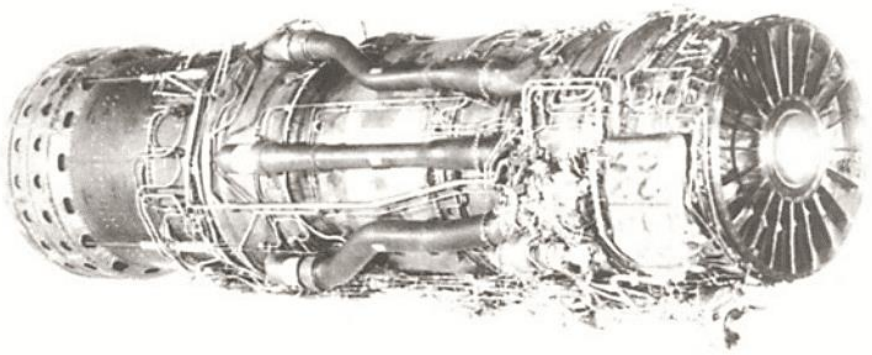

Figure 8: Pratt & Whitney J58 Turbojet [5]

The J58 operated as an afterburning turbojet engine until reaching speeds of a higher Mach number, after which flow redirected, bypassing the turbojet, to act as a ramjet engine with an afterburner [5]. This advancement propelled the application of VCEs for future combat aircraft, rather than having a commercial application. As technology advances and research enables a greater understanding of propulsion more advancements continue to be made with the VCE concept.

2.2.2 Present Variable Cycle Engine Technology

Recently GE Aviation has developed an engine for military applications. GE's XA100 is said to improve thrust by 20%, improve fuel consumption by 25%, and extend range by 30% [1]. This engine is made with the most heat resistant materials. In 2014 the engine was tested for the first time, and they were able to achieve the highest combined compressor and turbine temperatures in history [1].

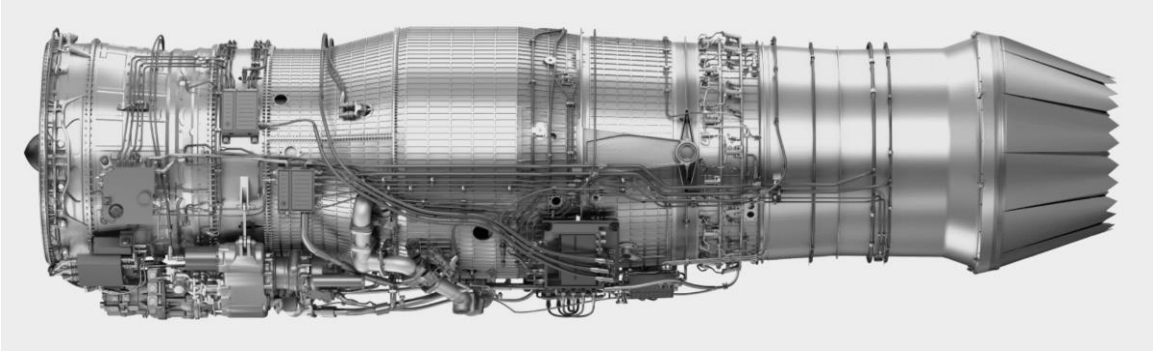

Figure 9: General Aviation XA100 Engine [1]

2.3 Sub-scale Variable Cycle Turbojet/Turboprop

All research has been directed toward the development of these engines at a large scale. There is little research being done or literature available when it comes to developing a VCE at a small scale. The reason for this might be related to the already difficult challenges faced with integrating bypass methods into the engine itself. Oklahoma State University is a current source of research on the topic of a sub-scale, variable cycle engine. A few years ago, this concept was slightly researched. The research mostly focused on propeller placement, pusher or tractor prop, and acoustics [7]. This current research is less interested in the acoustics of the engine. However, the setup and feasibility of the two different propeller methods has provided great insight. In the early stages of design, a pusher prop was the first concept.

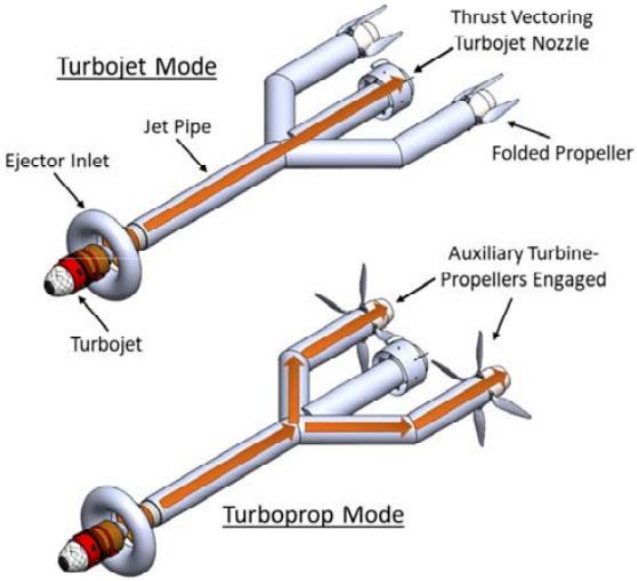

Figure 10: 1st Pusher Prop Concept [3]

The idea here shows multiple modifications to the original engine. This concept was quickly dismissed due to insufficient head pressure needed to drive the turbine after incorporating secondary flow. The effect of an ejector tube was quickly discarded. The conclusion from this result was that the turbine driving the propeller needs to be directly coupled to the initial exhaust from the engine. KingTech's development of the K45-TP allowed for a new pusher concept to created.

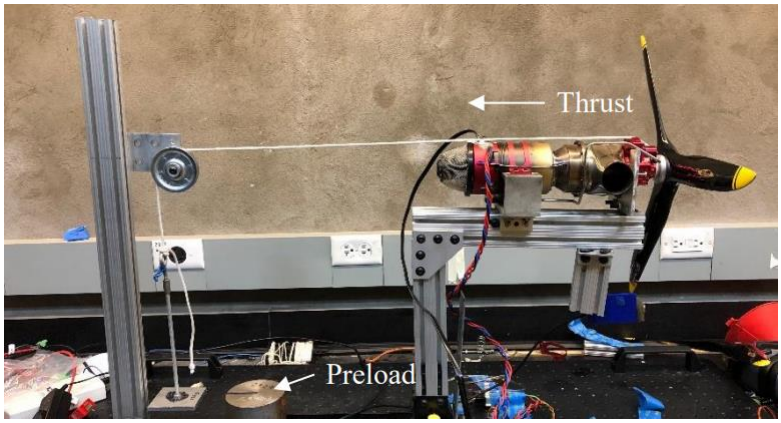

Figure 11: 2nd Pusher Prop Concept [3]

The second design of the pusher prop is much more practical. It eliminates all the addition weight that could be had from the first concept. In addition to this new concept, assembly is very versatile and simple. A variety of propellers could be used for this design. Installing and removing the propellers also makes this design favorable over the first. One crucial problem with this design was quickly realized. To get the thrust produced from turbojet mode, exhaust pipes must be directed towards the propeller. If not situated properly, the exhaust from turbojet mode could damage the propeller. Also, if in turboprop mode, the exhaust could still have damaging effects on the propeller. The final concept is a tractor prop configuration.

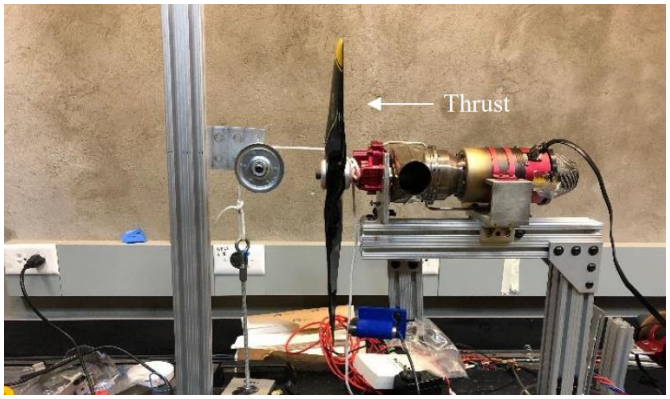

Figure 12: Tractor Prop Concept [3]

The tractor configuration eliminates the issue of exhaust damaging the propeller all together. It also has all the same benefits of the second pusher concept regarding the easy of assembly and versatility. The tractor prop configuration was the concept used for the research done in this experiment. The concept of a VCE between a turboprop and a turbojet at the small scale may mitigate some of the design challenges that come with the VCE at a large scale. However, there are still plenty of challenges to overcome with the purposed concept.

2.4 Parametric Cycle Analysis (PCA) for Turbojet

A PCA of a real engine from Mattingly uses thermodynamic relations to predict performance of gas turbine engines [5]. For a PCA a few common assumptions are made. We assume the flow is at steady-state and one dimensional, the gas is perfect, and the nozzle is perfectly expanded. Engine station numbers are used in a PCA to help identify pressures and temperatures at various places in the engine.

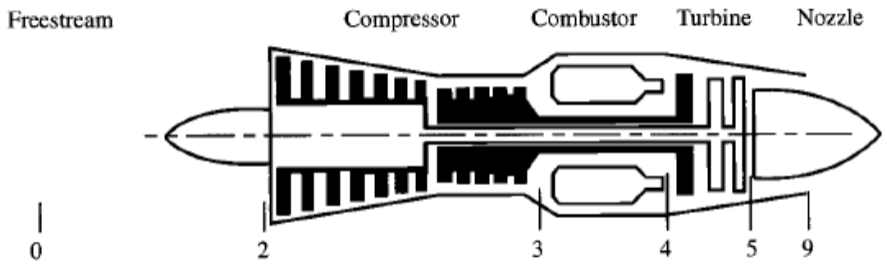

Figure 13: Turbojet with Station Numbers [5]

Figure 13 is a representation of a turbojet with the correct station numbers. The temperature after the combustor would be referred to as T_{t4}. If one in interested in the pressure ratio across a specific component it is denoted by π, while a temperature ratio across a component is denoted by τ. For instance, the pressure ratio across the compressor is π_c (pressure across combustor is

π_b) which is equal to P_{t3}/P_{t2}. In this study PCA will be used to model a smaller single spool turbojet. Primary inputs for a PCA are a flight condition Mach number, pressure, and temperature (M_0, P_0, T_0), compressor pressure ratio and turbine inlet temperature. With the flight conditions and the compressor pressure ratio total temperatures on both sides of the compressor can be found using the following equations:

$$\frac{T_{t0}}{T_0} = 1 + \frac{\gamma_c - 1}{2} * M_0^2 \quad (1)$$

$$\frac{P_{t0}}{P_0} = \left(\frac{T_{t0}}{T_0}\right)^{\frac{\gamma_c}{\gamma_c - 1}} \quad (2)$$

$$T_{t2} = T_{t0} \quad (3)$$

$$\frac{T_{t3}}{T_{t2}} = \pi_c^{\frac{\gamma_c - 1}{\gamma_c e_c}} \quad (4)$$

$$T_{t3} = \frac{T_{t3}}{T_{t2}} T_{t2} \quad (5)$$

Applying the first law of thermodynamics to the burner and dividing by the mass flow rate of the air, the fuel to air ratio can be solved for:

$$f = \frac{c_{pt} T_{t4} - c_{pc} T_{t3}}{\eta_b h_{PR} - c_{pt} T_{t4}} \quad (6)$$

The next step of the PCA is to perform a power balance between the compressor and the turbine to solve for the turbine exit temperature (mass flow rate of fuel is assumed negligible):

$$c_{pc}(T_{t3} - T_{t2})\eta_{mech} = c_{pt}(T_{t4} - T_{t5}) \quad (7)$$

Exit properties are found with the ratio of total pressure to static pressure at the exit and assuming no total temperature loss after the turbine:

$$\frac{P_{t9}}{P_9} = \frac{P_{t0}}{P_0}\pi_d\pi_c\pi_b\pi_t\frac{P_0}{P_9} \tag{8}$$

$$T_{t5} = T_{t9} \tag{9}$$

$$\frac{T_{t9}}{T_9} = \frac{P_{t9}}{P_9}^{\frac{\gamma_t - 1}{\gamma_t}} \tag{10}$$

Assuming that the nozzle is perfectly expanded, P_9/P_0 = 1. With this the exit velocity and specific thrust can then be solved for using:

$$V_9 = \sqrt{(T_{t9} - T_{t0}) * 2 * g_c * c_{pt}} \tag{11}$$

$$\frac{F}{\dot{m}_0} = \frac{(1+f)V_9 - V_{pursuit}}{g_c} \tag{12}$$

Lastly, SFC can be calculated by:

$$SFC = \frac{f}{F/\dot{m}_0} \tag{13}$$

The flight condition selected was 150mph at 2000ft the flight conditions selected are referenced from recent small turbine engine experiments [7],[8]. The compressor pressure ratio was estimated using data from other small turbine engines and recent experiments [2],[7]. The equations and steps process were referenced from Mattingly. Level of technology (LOT) is also used in a PCA to determine several other figures of merit for specific components. The figure below taken from Mattingly has specific values highlighted to represent what was used in the PCA for this experiment.

Component	Figure of merit	Type[a]	Level of technology[b] 1	2	3	4
Diffuser	$\pi_{d\,max}$	A	0.90	0.95	0.98	0.995
		B	0.88	0.93	0.96	0.98
		C	0.85	0.90	0.94	0.96
Compressor	e_c		0.80	0.84	0.88	0.90
Fan	e_f		0.78	0.82	0.86	0.89
Burner	π_b		0.90	0.92	0.94	0.95
	η_b		0.88	0.94	0.99	0.999
Turbine	e_t	Uncooled	0.80	0.85	0.89	0.90
		Cooled		0.83	0.87	0.89
Afterburner	π_{AB}		0.90	0.92	0.94	0.95
	η_{AB}		0.85	0.91	0.96	0.99
Nozzle		D	0.95	0.97	0.98	0.995
	π_n	E	0.93	0.96	0.97	0.98
		F	0.90	0.93	0.95	0.97
Mechanical shaft	η_m	Shaft only	0.95	0.97	0.99	0.995
		With power takeoff	0.90	0.92	0.95	0.97
Maximum T_{t4}		(K)	1110	1390	1780	2000
		(R)	2000	2500	3200	3600
Maximum T_{t7}		(K)	1390	1670	2000	2220
		(R)	2500	3000	3600	4000

Figure 14: Level of Technology Values [5]

Table 2 contains the values used to perform the PCA, detailed calculations using these values and equations can be seen in the Appendix.

Table 2: PCA Inputs

$V_{pursuit}$	190 mph	π_n	0.98	γ_t	1.36
Altitude	2000 ft	$\pi_{d,max}$	0.96	c_{pc}	0.24
π_c	2.1	e_c	0.88		
T_{t4}	1400 F	e_t	0.89	c_{pt}	0.275
π_b	0.92	η_{mech}	0.99		
η_b	0.94	γ_c	1.4	h_{PR}	18400

Using the results from the PCA another analysis was done to size several nozzles by using mass flow parameter:

$$MFP = \frac{\dot{m}}{A} * \frac{\sqrt{T_t}}{P_t} \tag{14}$$

Given that the engine in use is not a pure turbojet a variety of nozzles were designed based on the losses assumed from the configuration. There is a turbine directly behind the turbojet exhaust and when the propeller is locked it is uncertain what happens to the flow going throw that turbine. The jet exhaust flow is then bifurcated and turned 180 degrees so that it is facing the front of the engine and exhaust is now going in the opposite direct of the inflow. With this taken into consideration, nozzles were sized assuming zero percent loss of flow energy up to a forty percent loss of flow energy. The exit area of the exhaust without nozzles is just over 1.75 inches.

2.5 PCA for Turboprop

Turboprop engines usually have two spools: the core engine spool and the power spool. Reference the bottom schematic in Figure 3. The K45-TP is different from the conventional turboprop though. It has a turbine aft of the nozzle, rather than the turbine, which drives an 8:1 step down gear box that drives the propeller. Locking the propeller enables the exhaust to exit past the turbine and through the modified exhaust system producing jet trust. When analyzing a turboprop, it is more appropriate to consider the work done by the engine rather than thrust produced. Work output coefficient (C) is defined by the power interaction or mass flow of the air through the core of the engine over the enthalpy of the freestream of the air. For the thrust of the core stream work output coefficient is defined as:

$$C_{core} = \frac{F_C V_0}{\dot{m}_0 c_P T_0} \tag{15}$$

Likewise, the coefficient for the propeller is:

$$C_{prop} = \frac{\eta_{prop} \dot{W}_{prop}}{\dot{m}_0 c_p T_0} \tag{16}$$

Adding the two together provides us with the total work output coefficient:

$$C_{tot} = C_{core} + C_{prop} \tag{17}$$

The PCA for a turboprop engine is very similar to the turbojet PCA except for the low-pressure turbine that drives the propeller. Rather than performing a power balance between the compressor and the turbine, the power out of the low-pressure turbine is equated to the power into the propeller:

$$\eta_{mL}\dot{m}_{4.5}c_{pt}(T_{t4.5} - T_{t5}) = \frac{\dot{W}_{prop}}{\eta_g} \tag{18}$$

η_g is the gearbox efficiency, this must be known along with mechanical efficiency and can change depending on the level of technology being used. Specific thrust and specific power are a couple of key parameters to look when analyzing a turboprop:

$$\frac{\dot{W}}{\dot{m}_0} = C_{tot}c_{cp}T_0 \tag{19}$$

$$\frac{F}{\dot{m}_0} = \frac{C_{tot}c_{cp}T_0}{V_0} \tag{20}$$

Specific fuel consumption is defined differently as well. When dealing with propeller driven aircraft it is more common to refer to it as power specific fuel consumption:

$$S_p = \dot{m}_f/\dot{W} \tag{21}$$

2.6 Propeller Theory

Propellers are typically characterized by the amount of torque and thrust they produce at a given RPM, and by the ratio of the power transferred to the air versus the mechanical power, known as propeller efficiency [14],[15], and [16]. As is typical in aerodynamics applications, the

dimensional thrust and power are not typically specified; rather, non-dimensional coefficients are presented to allow the end-user of the data to adapt the results to their application, i.e., operating with a different atmospheric density or at a different velocity. Unlike aircraft or wing aerodynamics, propeller performance coefficients are not non-dimensionalized using freestream velocity. This is to accommodate how Reynolds number effects are seen by the propeller, as in the propellers frame of reference, chord-wise velocity at a given radial location is a function of both freestream and rotational velocity. Reynolds number is defined as the ratio of momentum force and viscous shear force. For propellers, Reynolds number is based on chord length (c), relative velocity ($Vrel$), air density (ρ), and dynamic viscosity (μ). To satisfy the objective of the research, testing was conducted at low Reynolds numbers. Relative velocity is a result of the freestream velocity coming into the and the rotational velocity from the propeller.

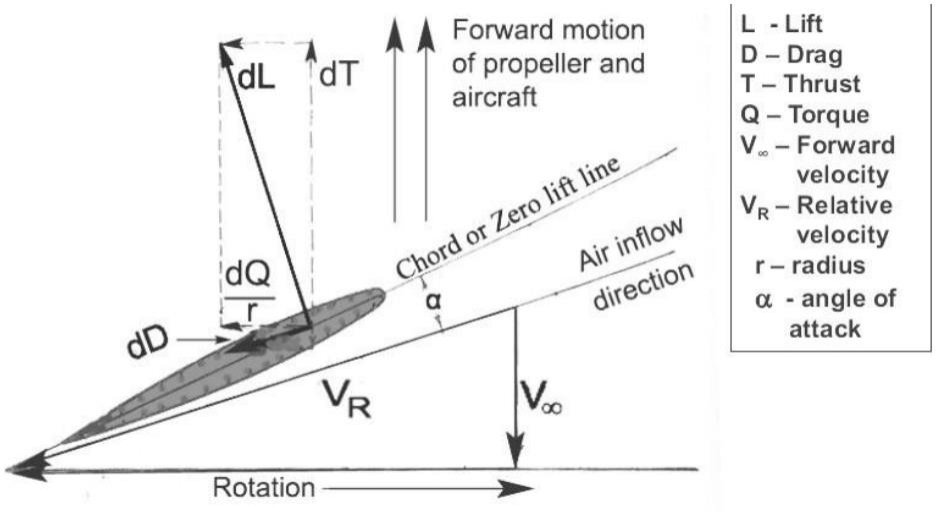

Figure 15: Diagram of Propeller Nomenclature [16]

$$R_e = \frac{\rho c V_{rel}}{\mu} \tag{22}$$

Propeller characteristics are typically cataloged as a function of the ratio between freestream and angular velocity to allow for translation to arbitrary operating speeds. This ratio is known as the advance ratio (J), which is shown symbolically in Equation 23, where V is the freestream velocity, n is the rotational frequency in revolutions per second, and D is propeller diameter.

$$J = \frac{V}{nD} \tag{23}$$

Given the definition of advance ratio, the thrust coefficient can be defined as shown in Eq. 24. This non-dimensional quantity relates thrust produced (T) to the rotational velocity (n) and propeller diameter (D), where ρ is the density of the air the propeller is acting on.

$$C_t = \frac{T}{\rho n^2 D^4} \tag{24}$$

Similarly, power is a non-dimensional quantity that relates power (P) to the density of the air (ρ), the rotational velocity (n) and propeller diameter (D), as in Eq. 25.

$$C_p = \frac{P}{\rho n^3 D^5} \tag{25}$$

Finally, propeller efficiency is the ratio power transferred to air to mechanical power required to turn the propeller, which is calculated with the expression in Eq. 26.

$$\eta_p = \frac{J * C_p}{C_t} \tag{26}$$

2.7 Mission Analysis

Using the notional mission from Figure 16 and installation losses of 5%, an analysis according to Mattingly [4] was conducted to study the impact of a variable-cycle engine on a UAS range and endurance. Figure 17 shows a benchmark aircraft that was used for aerodynamic elements of the analysis, and Figure 16 also shows the numbers for the mission legs.

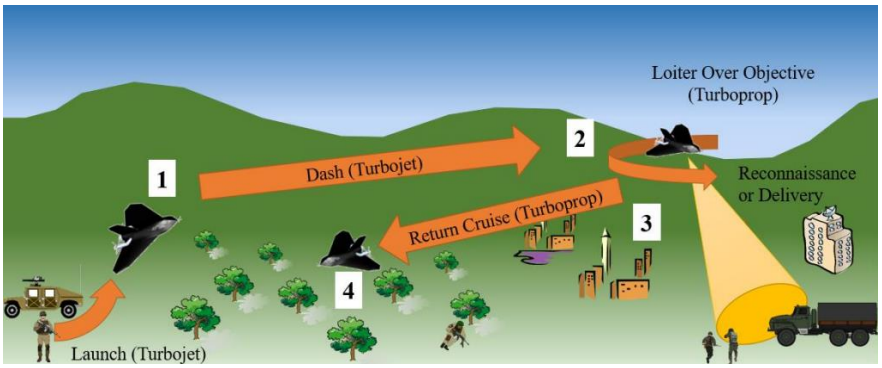

Figure 16: Notional Mission Legs for Dual-Mode Engine [3]

Figure 17: Notional Aircraft for Dual-Mode Engine

Primary inputs for the mission analysis include aircraft characteristics, engine SFC, flight condition and desired range of the first leg. SFC for the turbojet (dash) leg of the mission used the results from the PCA (π_n LOT 3). The SFC for the turboprop legs used a partial throttle

estimate for the K45TP turboprop [9]. For the mission analysis calculations, lift was assumed to equal weight for all mission legs therefore:

$$C_L = \frac{2Wt}{\rho_0 V^2 S} \tag{27}$$

$$C_D = C_{D0} + KC_L^2 \tag{28}$$

W is defined as the weight of the aircraft at a particular mission leg, and V is the velocity at a certain mission leg. S is the wing area. The Breguet range equation was used to solve for fuel burn during mission legs and loiter time.

$$R = \frac{V}{g}\frac{1-\Phi}{SFC}\frac{C_L}{C_D}\ln\frac{W_{t1}}{W_{t2}} \tag{29}$$

Where Φ is the installation losses. The Breguet range equation was used without the velocity term for endurance of the loiter leg of the mission and was also used to solve for the change in aircraft weight (fuel burn) given a range to dash. A summary of assumed values can be seen in Table 3.

Table 3: Assumed Values for Mission Analysis

V (dash)	150mph	C_{d0}	0.013
Altitude	2000 ft	AR	22.5
W (empty)	13lbf	M (loiter)	0.05
W (fuel)	6lbf	$W_{factor4}$	1.02
S	$2.5ft^2$	Φ	5%
SFC dash	$\frac{2.29}{hr}$	SFC_{2-4}	$\frac{1}{hr}$

Detailed calculations can be found in the Appendix. Length of loiter when given an initial cruise range is the focus of the mission analysis. The results of the mission analysis highlight the tradeoff between loiter endurance and range capability of the dash leg. A mission that requires as much loiter endurance as possible can achieve about 35 minutes of loiter if the range is kept at 10 miles. SFC was 2.29 lbf/lbm/hr for the entire turbojet mission and 1 lbf/lbm//hr for the entire turboprop mission. Mission analysis results show less loiter time at all points for the turbojet mode when compared to a dual-mode mission. The turbojet envelope features a similar negative correlation in loiter endurance as dash range is increased. Turboprop-only loiter endurance decreases more quickly with increased range. Although the turboprop has a much lower TSFC, total fuel used on the dash/cruise legs increases significantly with range because of the low flight speed. This leaves significantly less fuel for the loiter leg with increasing range. In addition to better range and endurance in general, the variable-cycle engine also has the advantage of dash in the first leg. These results show the effectiveness of a variable-cycle engine on a diverse mission involving dash, loiter and low-speed return cruise.

2.8 Corrected Thrust

Corrected performance parameters allow for data taken under one set of conditions to be extended to other conditions. There are several reasons for using corrected engine and component performance parameters. It is impossible to accumulate experimental data for the large number of possible operating conditions, and it is often impossible to reach many of the conditions in a single, affordable test facility [5]. Corrected parameters allow for comparison of engine performance operated at different test facilities with different atmospheric conditions [5]. The corrected performance highlighted in this paper will be corrected thrust and corrected SFC. Dimensionless pressure and temperature coefficients, represented by δ and θ will be calculated

based on the actual pressures and temperature recorded at the time of testing. Equations used to get the dimensionless coefficients are:

Pressure:

$$\delta_i = \frac{P_{ti}}{P_{ref}} \tag{30}$$

Temperature:

$$\theta_i = \frac{T_{ti}}{T_{ref}} \tag{31}$$

They are then applied to thrust to get corrected thrust as follows.

Thrust:

$$F_c = \frac{F}{\delta_0} \tag{32}$$

CHAPTER III

METHODOLOGY

3.1 Nozzle Design

After performing a PCA for the turbojet engine, a nozzle exit velocity of 1234.3 ft/s was found. This gives us an exit Mach number of 0.612. Then using the graph below the respective MFP was using to then size the exit area for the nozzle.

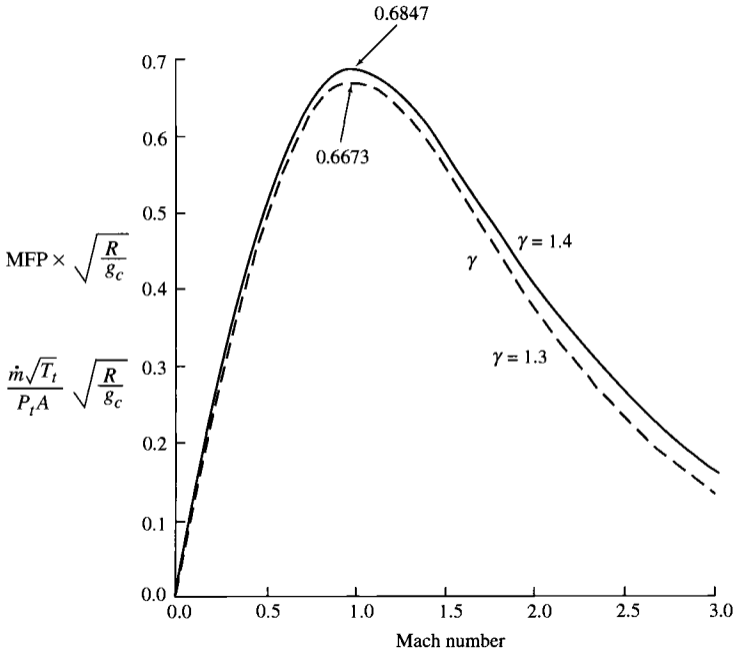

Figure 18: Mass Flow Parameter vs Mach Number [5]

As seen in the graph, with a Mach number slightly greater than 0.5 and assuming a gamma of 1.3 the chosen MFP value for sizing the nozzles is 0.5647. A desired nozzle exit area of 1.924 in^2 was found assuming approximately 10 lbf of produced thrust. These evaluations were made based on a PCA a pure K45 turbojet engine. The engine being used in the study is a K45-TP which has some modifications aft of the exhaust. The exhaust must travel past a fixed turbine, when in turbojet mode, that drives the propeller, and it is then bifurcated. Without CFD it is difficult, but CFD is also not conclusive. Because of this a variety of nozzles with varying exit sizes were designed and fabricated. In total five different nozzle sizes were tested. There sizes range from 1.7 in^2 to 0.75 in^2. The diameter of each nozzle exit was found and then converted to millimeters for ease of creating the nozzles in Solidworks. The nozzle exit diameters include 1.575-in, 1.417-in, 1.260-in, 1.102-in, and 0.945-in. The nozzles are in the shape of a frustrum, so I designed the frustrum using the aid of an online resource, hampsonlife. Hampsonlife asks for three different inputs to determine the remaining geometry for the frustrum. The three inputs are base diameter, top diameter, and height. The base diameter input was 1.969-in and the height was 1.772-in. The top diameter included the five mentioned earlier. After all the remaining dimensions were solved for and then the nozzles were designed in Solidworks. In the figure below the results of the nozzle frustums can be seen in the figure below.

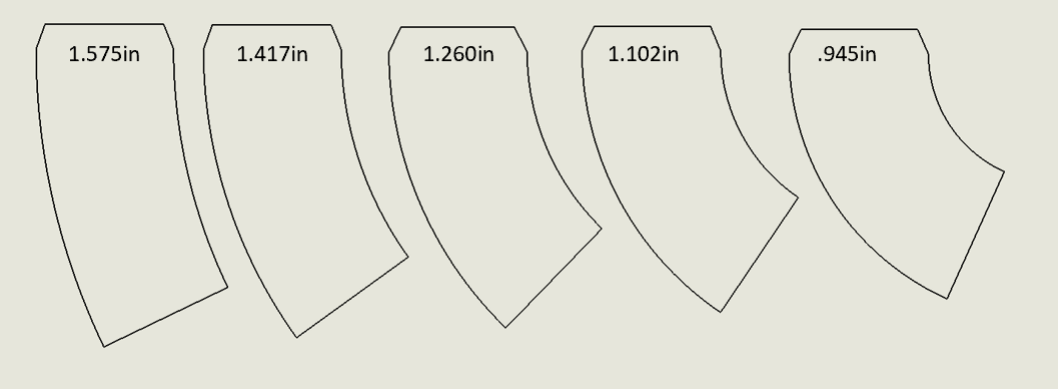

Figure 19: Nozzle Frustrums

Two of each of the drawings of the nozzles were cut out of 35-gauge sheet metal using an abrasive water jet provided by OSU North Campus Labs, Design and Manufacturing Lab. Once all the cutting was completed the 2D cutouts were rolled to make the welding process easier.

Figure 20: Sunkko 737G+

In Figure 19 the Sunkko 737G+ can be seen. This is the device used to complete the manufacturing process for all the nozzles.

Figure 21: Complete Nozzles for Testing

The next and final step in completing the nozzles was to develop a way to mount them to the test stand. The main challenge with the design was figuring out how to make the nozzles easily removeable to make changing them out for a different size quick and efficient. This design will be discussed later in the methodology section.

3.2 Test Stand Design

Because of the comparisons among different types of propulsion systems, a versatile, custom stand for measuring thrust was desired. The test stand was created in such a way as to measure thrust in both configurations along the same axis. The load cell was mounted in front of the engine inlet on separate fixed platform. The engine was mounted along the same axis but can slide forward and backward along a single track. Figure 22 below shows a general schematic of the entire setup. Figure 23 is the actual completed test stand.

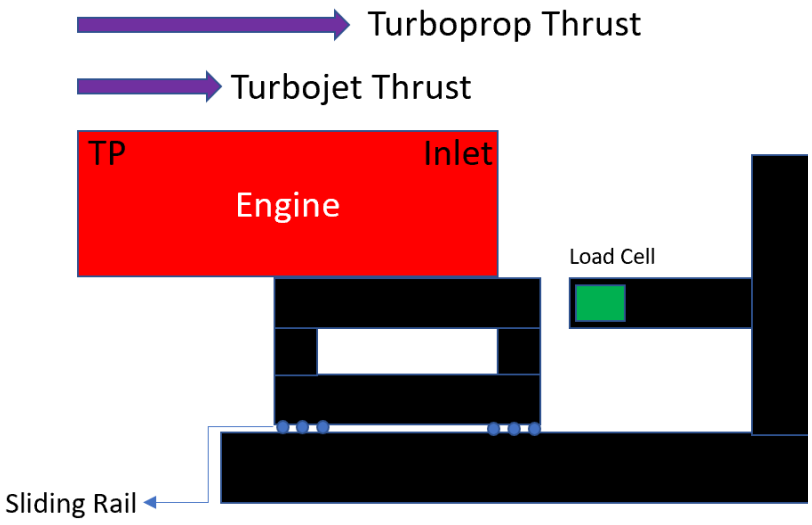

Figure 22: Test Stand Measurement Set-up Diagram

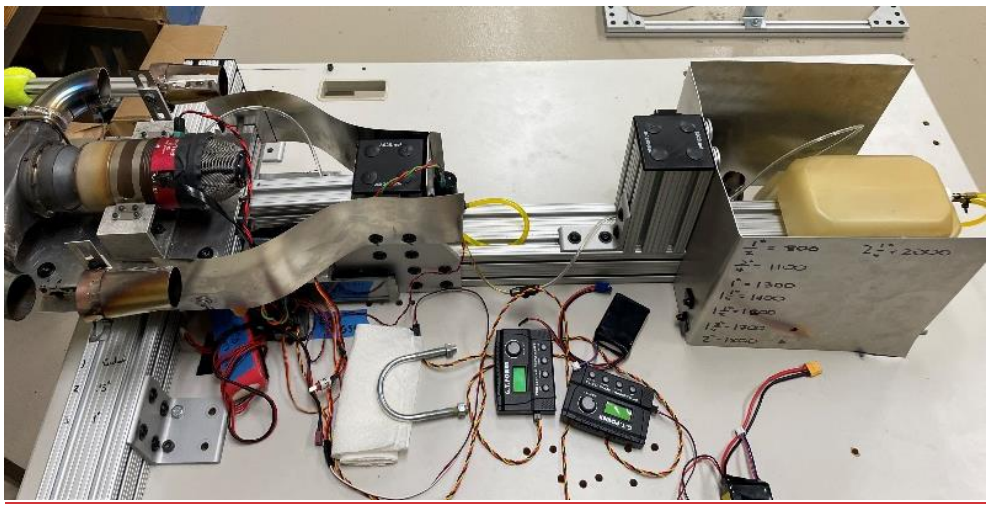

Figure 23: Completed Test Stand

From the picture above is can be seen that there are two different sections to the whole test stand.

3.2.1 Engine Mount and Platform

The engine mount itself was the most difficult thing to design for this test stand. There were several major design challenges that involved incorporating components crucial to the proper functionality of the testing system. The first component that needed to be properly installed was a sliding rail that the engine and engine mount would rest on. The purpose of the sliding rail is to enable the engine to move back and forth freely along a linear axis.

Figure 24: Engine Platform Sliding Rail

The reason the engine needs to be able to move freely is to enable the load cell to take data. The load cell used for this experiment was a Futek LSM300 OEM load cell. This load cell is also known as the belt buckle load cell. It records both tensile and compressive forces, but for obvious reasons for this experiment force is only recorded in one direction. The figure below represents both the load cell and how it must be mounted.

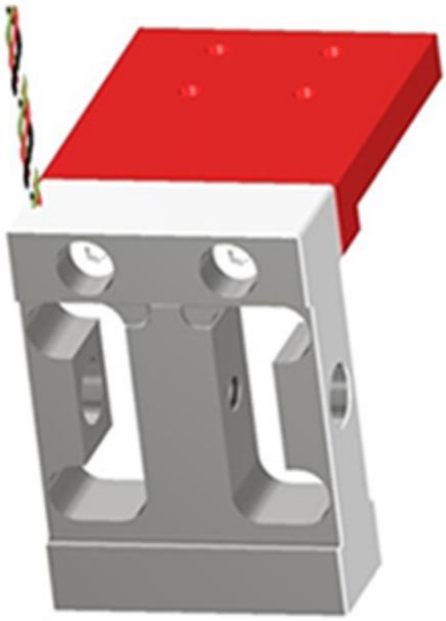

Figure 25: LSM300 Load Cell [4]

Table 4: Load Cell Performance Specifications

SPECIFICATIONS	
PERFORMANCE	
Nonlinearity	±0.02% of RO (2.2–100 lb) ±0.06% of RO (200 lb)
Hysteresis	±0.02% of RO (2.2–100 lb) ±0.06% of RO (200 lb)
Nonrepeatability	±0.02% of RO
Creep	±0.025% of Load

This method of mounting the load cell was cause for a very large design constraint and came with a couple challenges. First, the load cell had to be fixed to a separate platform to ensure proper mounting to record accurate data. Second, the load cell had to be connected to the engine platform to be able to record both jet thrust, and propeller thrust. To mount the load cell to the fixed platform, a piece of 1.5-in single slot t-slot aluminum was attached to the left tower. The left tower can be seen to the right of the engine itself in Figure 26. This t-slot aluminum had two

holes drilled into it allowing for the load cell to be fixed to it. The figure below shows the completed design for the load cell mount.

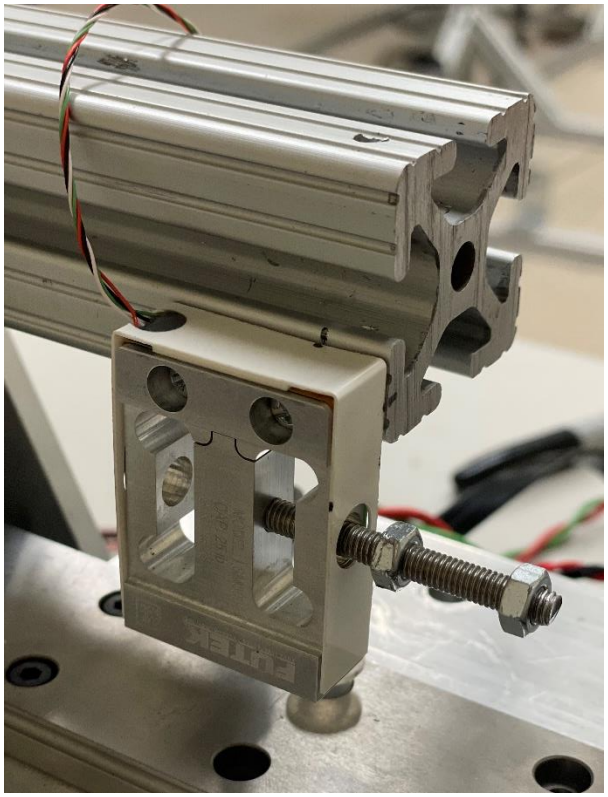

Figure 26: Load Cell Mount

After completing the load cell mount, a few modifications had to be made to the engine platform to connect the whole test system together. On the inlet side of the engine platform another piece of t-slot aluminum was place perpendicular to the piece of t-slot in the figure above. The t-slot on the engine platform is sandwiched between two pieces of stainless-steel sheet metal. The bottom sheet is mounted to the slider as mentioned earlier. While the top sheet has the engine itself mounted to it. The t-slot sandwiched between the two steel sheets also had a hole drilled through it. Having this hole in the t-slot enabled the threaded rod attached to the load cell, as seen in the figure above, to slide through and connect the whole system together. The two hex nuts which

can also be seen in the figure above were tightened down on both sides of the t-slot to ensure that it was secure. The figure below shows the completed method for attaching the load cell to the engine platform.

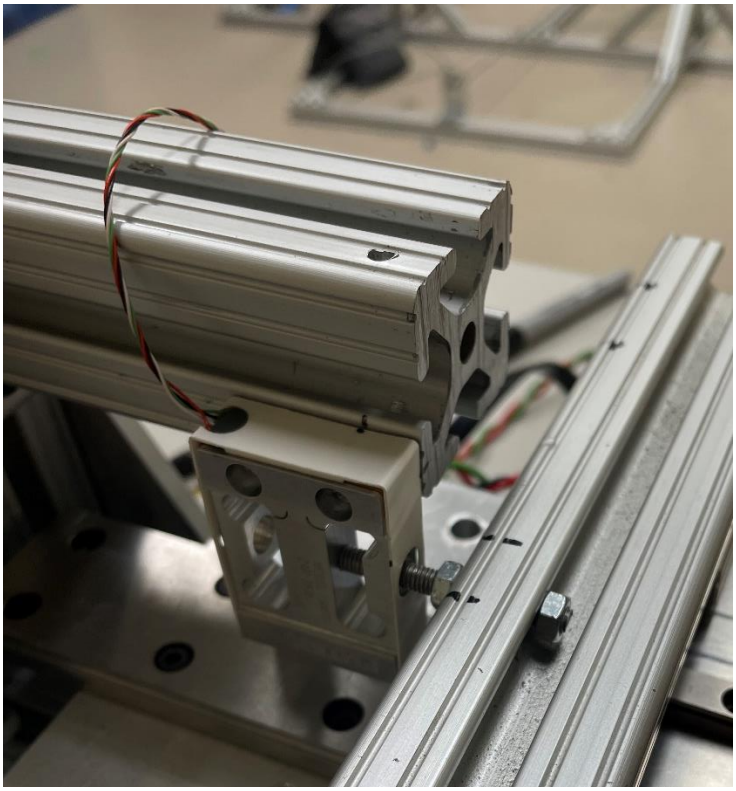

Figure 27: Load Cell Attached to Engine Platform

The next challenge for the engine platform was designing a method to incorporate the nozzles in such a way that they can be moved closer to and farther from the engine exhaust while the engine is running. This overall design required five major components. The first, is a custom bracket the nozzles themselves attach to. The brackets for the nozzles ensure that the nozzles are completely secure and do not shift or move while the engine is running. From there an additional couple of brackets had to be designed. The purpose of the second set of brackets is to mount the nozzles on their respective brackets on and connect them to a sliding rail. Which brings up the next

component for the nozzle system. The sliding rail has the brackets holding the nozzle brackets mounted to it. The sliding rail enables the nozzles to move freely, closer to and farther from the engine exhaust pipes. The nozzles also slide on the same axis as the engine itself. The fourth component crucial to the nozzle system is an INJORA RC servo 70kg super torque digital motor with a 15T metal arm. The servo motor allows the nozzles to be moved closer and farther remotely with the aid of a G.T. power professional servo tester. The final component of the nozzle system is a push rod. The push rod connects the servo motor to the sliding base. The push rod not only allows the whole system to be integrated together in a sleek fashion, but it also increases the range of motion that the nozzles can move. An additional modification had to made to the t-slot that hold the treaded rod connecting to the load cell. A large chunk of the t-slot had to be machined out of it to allow the push rod to move freely. The figure below represents the nozzle system, but the nozzles themselves are not installed.

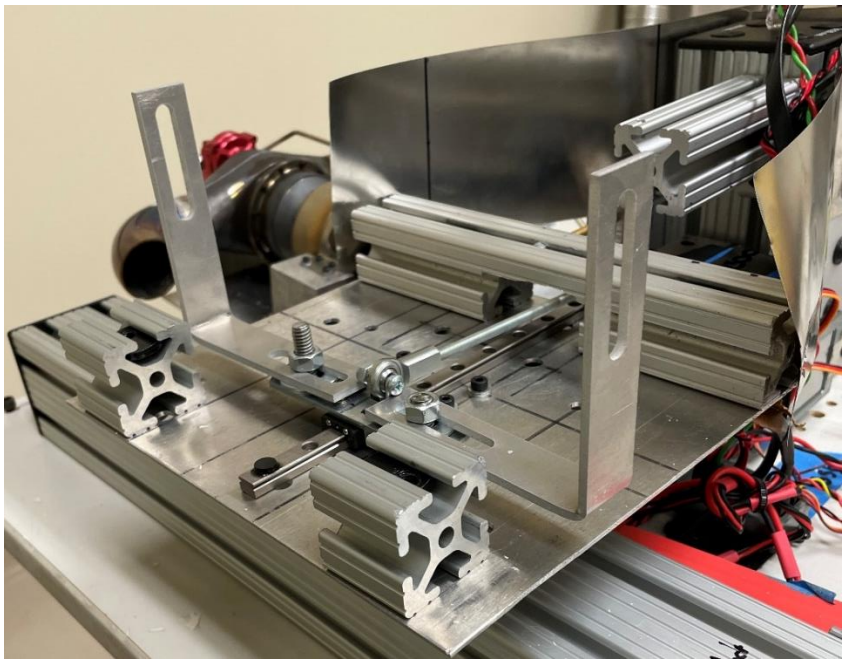

Figure 28: Nozzle System (nozzles not pictured)

The final component to the engine mount is a supporting mount place aft of the exhaust manifold that supports the propeller portion of the engine. The engine itself has a place for a mount to be installed, so the mount was largely designed around that. In the figure below the mounting piece already attached to the engine can be seen.

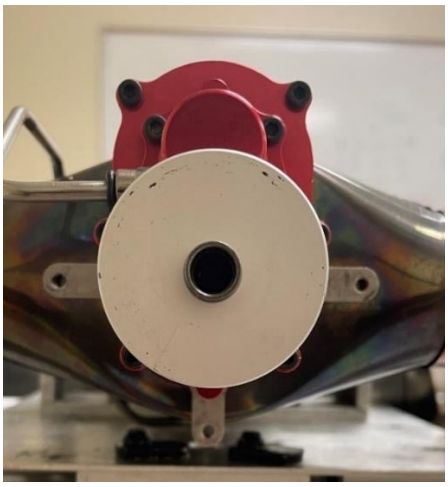

Figure 29: Engine Mounting Piece

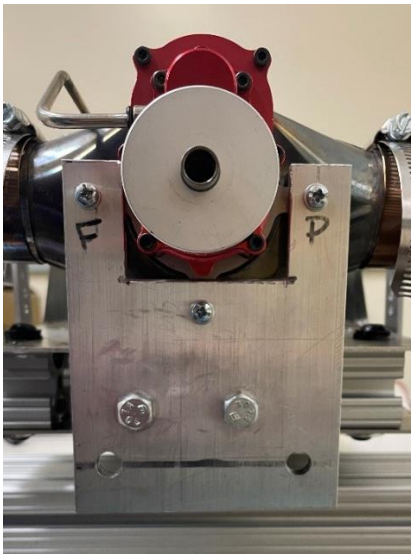

Figure 30: Supporting Mount Installed

The supporting mount was easy to manufacture. A piece 0.25-in thick aluminum was found and cut down to fit around the propeller. The final dimensions of the mounting piece are 3-in by 4-in and the slot dimension are 2-in by 1.5-in. And holes were drilled so that it could be properly attached to the engine itself. The propeller then placed on the propeller system and secured with 5/16-in bolt.

3.2.2 Fuel System Mount

The fuel system is a part of the first tower and the second tower. The fuel system includes a fuel pump, fuel filter, shut off valve, a fuel tank, and fuel line connecting it all together. On the first tower (see Figure 23 for reference), the fuel pump and the fuel filter are mounted and protected from any heat coming from the exhaust. The first tower is also the mount for the load cell. In addition to components of the fuel system and the load cell, the first tower also has a heat shield integrated into it. The heat shield serves to protect some of the engine electronics, and the load itself. The second tower (again see Figure 23) is placed farther to the right of the engine. The main purpose of the second tower is to be a mount for the fuel tank heat shield. This second heat shield protects the fuel tank for any exhaust coming from the engine. The heat shield also has strategic folds in it to reduce the amount of impact it may how on propeller wash from running the engine in turboprop mode.

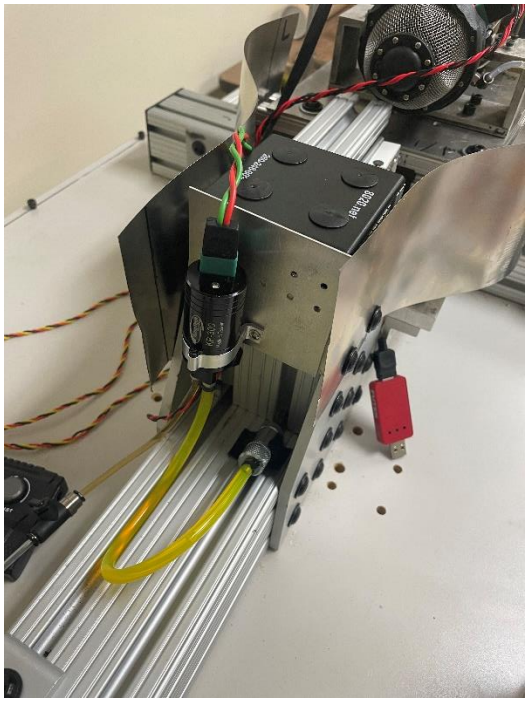

Figure 31: First Tower of Engine Stand

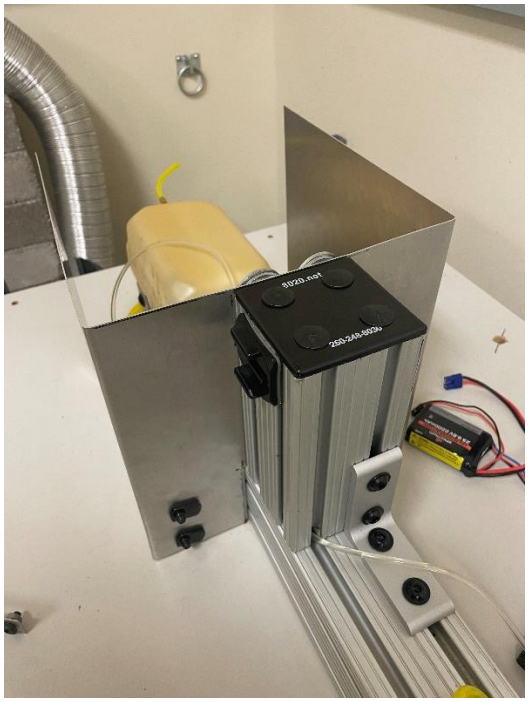

Figure 32: Second Tower of Engine Stand

3.3 Turbojet Configuration

When running the engine in turbojet mode the propeller must be locked or mounted in such a way that it is prevented from spinning. To do this, a U-bolt was integrated into the mount that supports the turboprop section of the engine. Padding was also placed around the propeller blade to minimize potential damage that could be induced to the leading edge of the propeller blade. This can be seen in Figure 33 below.

Figure 33: U-bolt Propeller Lock (missing padding)

In addition to locking the propeller, the variable distance nozzle mounts, as well as fixed nozzles had to be integrated into the test stand. The fixed nozzle mounts were simple, as they are welding to the exhaust pipe as seen below.

Figure 34: Fixed Nozzle Configuration (uninstalled)

The variable distance nozzles came with more design challenges. An additional sliding rail was acquired and placed underneath the engine in a gap between the two mounting surfaces. On the slider, a mount for brackets was placed as well as a small mount to connect a linear rod to a servo. A servo enables the nozzle brackets to be moved forward and backward with the aid of a G.T. power professional servo tester. The nozzles are capable of being backed off from the exhaust at a maximum distance of 2in, and minimum distance of 0.5-in. The setup can be seen in the figure below.

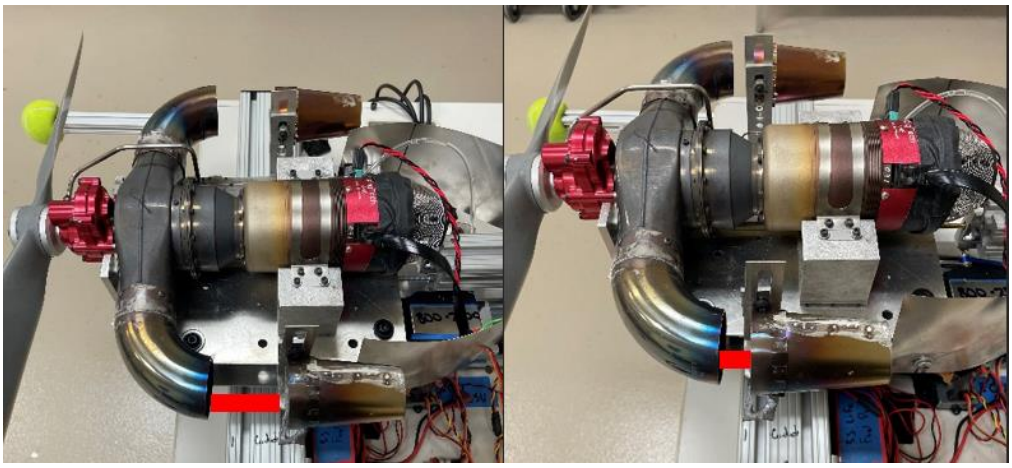

Figure 35: Nozzle Backoff Distances (left 2-in backoff, right 0.5-in backoff)

3.4 Turboprop Configuration

The turboprop configuration is near identical to the turbojet configuration. The only change is that the U-bolt is removed from the support mount to enable the propeller to spin freely.

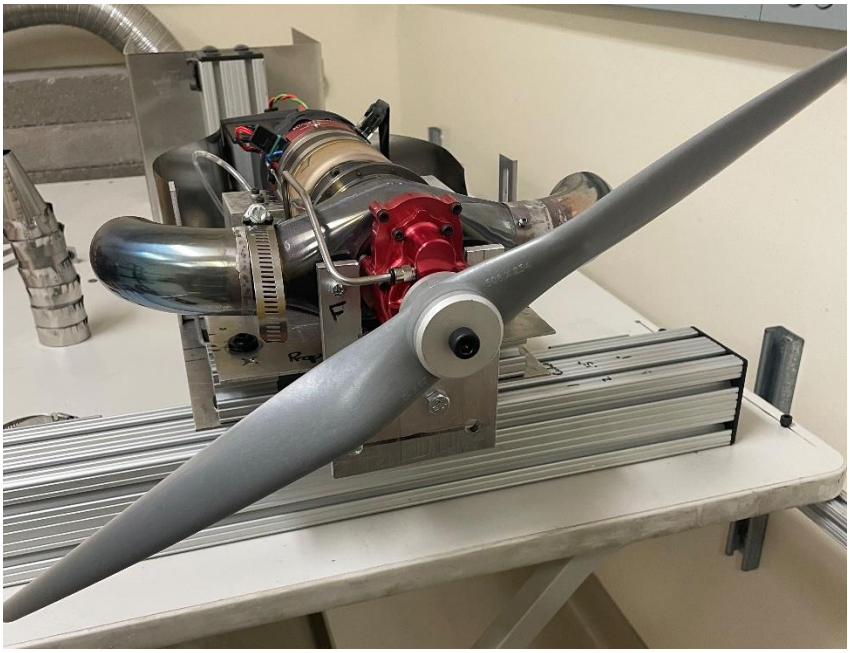

Figure 36: Turboprop Mode

3.5 Folding vs. Fixed Propeller Testing

Five different nozzles geometries were tested at seven distances, and one nozzle geometry was tested while fixed to the exhaust pipes. All configurations were tested in both turbojet mode and turboprop mode. There is a wide variety of different testing configurations. They include testing the each of the nozzles at five different distances while tracking the trend as the nozzle moves closer to the exhaust pipe. With an exit diameter of 0.945-in, 1.102-in, 1.260-in, 1.417-in, and 1.575-in measured 2-in from the exhaust pipe to 0.5-in from the exhaust pipe (in both turbojet mode and turboprop mode). And lastly nozzles with an exit diameter of 0.945in were fixed to the exhaust pipes (in both turbojet mode and turboprop mode). Rather than running two separate tests for each distance, the nozzles were moved closer to the exhaust pipe while the engine was running. This not only allowed for a more efficient testing procedure, conserving fuel, but also the effect of moving the nozzles closer can be seen as they get closer to the minimum backoff distance. Two X's means that this configuration was tested and measured in both turbojet mode and turboprop mode. One X means only turbojet mode was tested and measured.

Table 5: Testing Matrix

Exit Diameter	0.945-in	1.102-in	1.260-in	1.417-in	1.575-in
Backoff Distance					
2-in	X	XX	XX	XX	XX
1.75-in	X	X	X	X	X
1.5-in	X	X	X	X	X
1.25-in	X	X	X	X	X
1-in	N/A	X	X	X	X
0.75-in	N/A	X	X	X	X
0.5-in	N/A	XX	XX	XX	XX
Fixed	XX				

3.6 Folding vs. Fixed Propeller Testing

Tests were conducted in the OSU subsonic wind tunnel located in the Advanced Technology Research Center. The wind tunnel runs on a 125-hp draw down drive and has a 3-ft by 3-ft area test section. Wind tunnel flow velocity is measured using a pitot static probe attached to an Omega differential pressure transducer (Model PX653-02D5V). This wind tunnel has an operational dynamometer that was validated by Jdiobe et al. [14]. Angular speed is measured using a Hall-effect sensor, and a Futek MBA500 biaxial load cell is used to measure thrust and torque, as shown in Figure 37. Table 1 includes a summary of dynamometer electrical components and instrumentation.

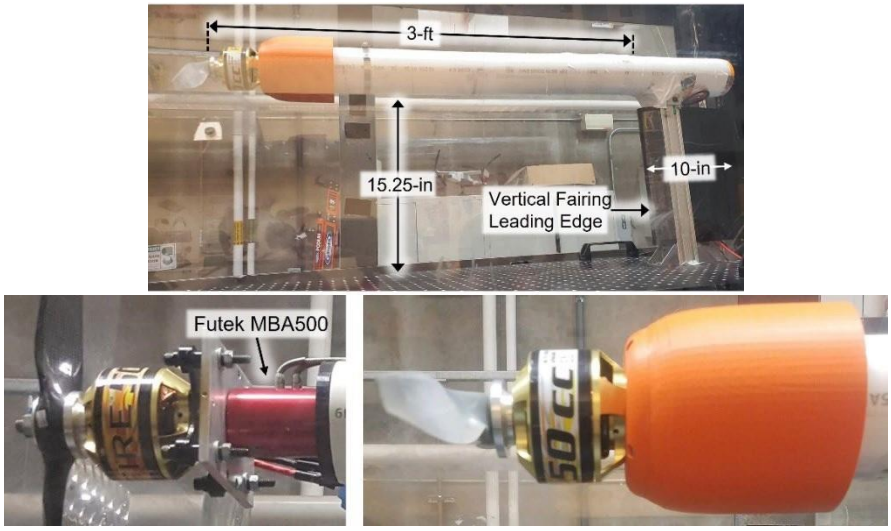

Figure 37: OSU Wind Tunnel Dynamometer

Table 6: Summary of Dynamometer Electrical Components and Instrumentation

COMPONENT	MANUFACTURER	MODEL	SPECIFICATIONS
Drive Motor	Great Plains	Rimfire 50CC	5-kW, 55-V, 230-Kv
DC Power Supply	Magna-Power	SL32-125/208 +LXI	4-kW, 32-V, 125-Amp
Electronic Speed Controller	Castle Creations	Phoenix Edge HV160	50-V, 160-Amp
Throttle Controller	GT Power	Pro Digital Servo Tester	7.4V to 12V DC input 4.8V output
Hall-Effect Sensor	Honeywell	SS460S	1.5 micro-sec rise-fall
Thrust-Torque Load Cell	Futek	MBA500	50-lb, 50-in-lb, Error 0.25% RO

Tests for propeller diameters 20-in fixed and folding at tunnel velocities ranging from 25 to 50-ft/s and propeller speeds ranging from 1,500 to 5,500 RPM. Procedures for these tests are as follows. First, mount the propeller to a dynamometer electric drive motor. Next, open Arduino software for displaying propeller RPM. After that, open Sensit software to tare instruments and adjust settings for autonomous testing to record thrust and torque. Then, turn on dynamometer electric drive motor power supply. Finally, turn on wind tunnel fan drive motor power and set test section speed to 25 ft/s. Set propeller speed to 1,500 RPM using servo tester and Arduino display. Visually read and manually record all displays, averaging five measurements for propeller RPM and power supply voltage and current. Run the Sensit software autonomous recorder for 10 seconds at 100 samples per second. Repeat these steps at propeller speeds ranging from 1,500 to 5,500 RPM. And then repeat all of those steps for wind tunnel air speeds ranging from 25 to 50 ft/s.

CHAPTER IV

RESULTS

4.1 Variable Nozzle Distance Turbojet Testing

The varying nozzle geometries were all tested in turbojet mode and turbojet mode and tested at distances of 2-in to 0.5-in. The engine was brought up to full throttle and then the nozzle distance was changed while data was being recorded. At each measuring distance, an allotted of 8 to 10 seconds was allowed for the engine to run at that backoff distance. Again, backoff distance is the distance between the nozzle and engine exhaust pipe.

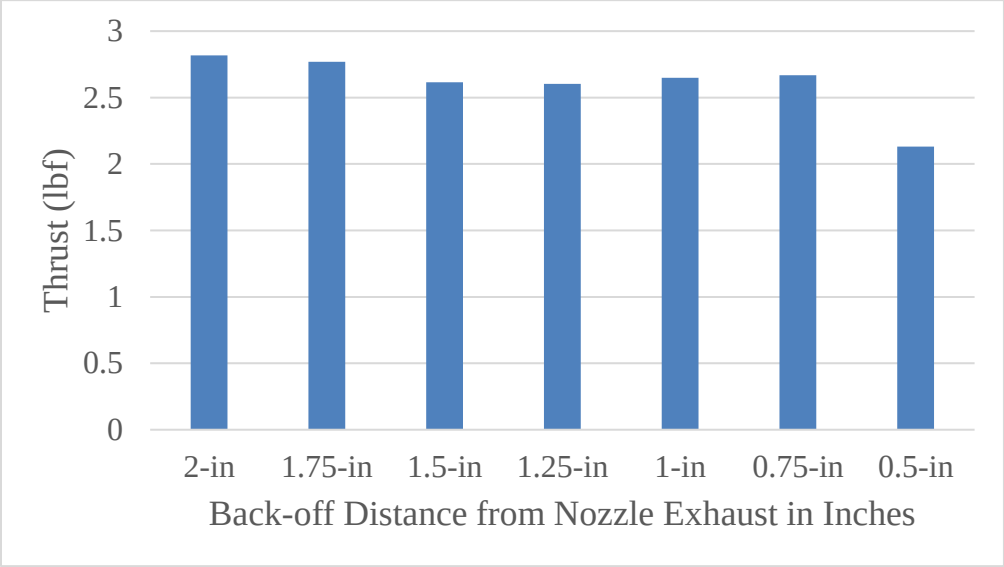

Figure 38: Jet Thrust vs Backoff Distance for 1.575-in exit diameter nozzle

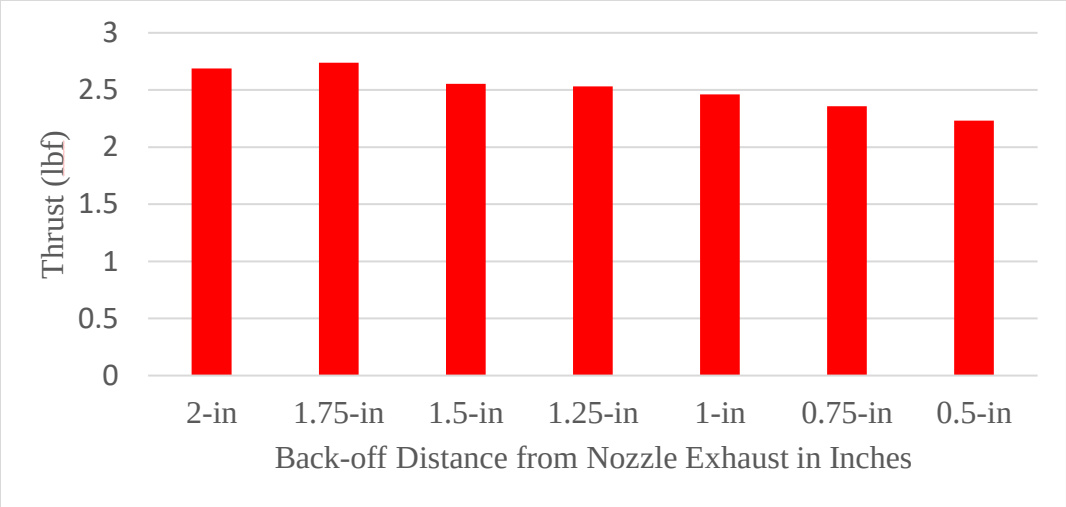

Figure 39: Jet Thrust vs. Backoff Distance for 1.417-in exit nozzle diameter

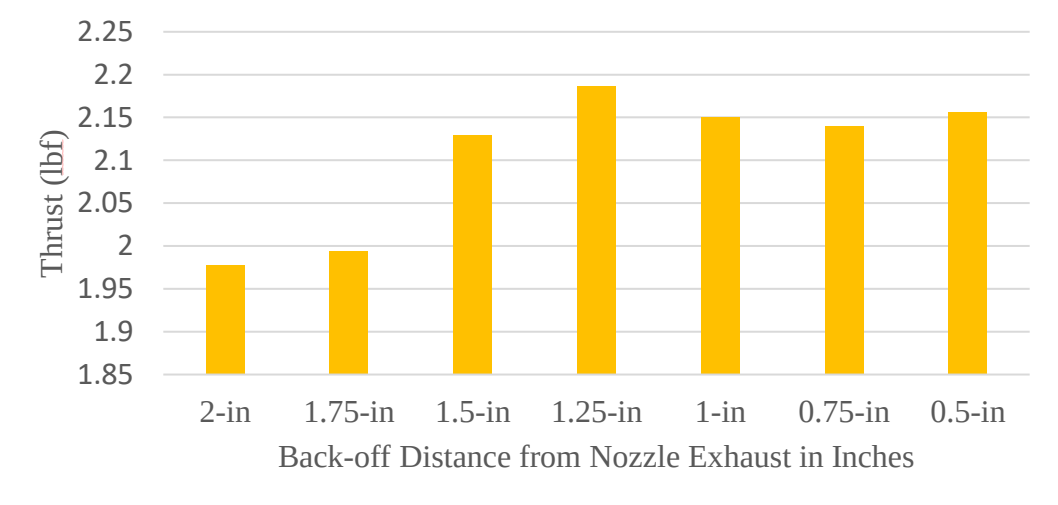

Figure 40: Jet Thrust vs Backoff Distance for 1.260-in exit nozzle diameter

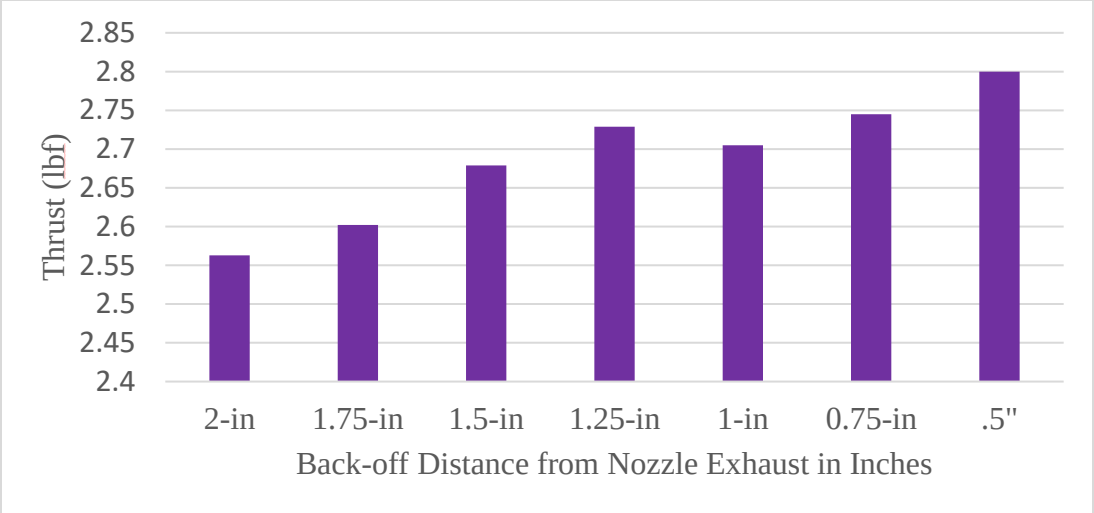

Figure 41: Jet Thrust vs Backoff Distance for 1.102-in exit nozzle diameter

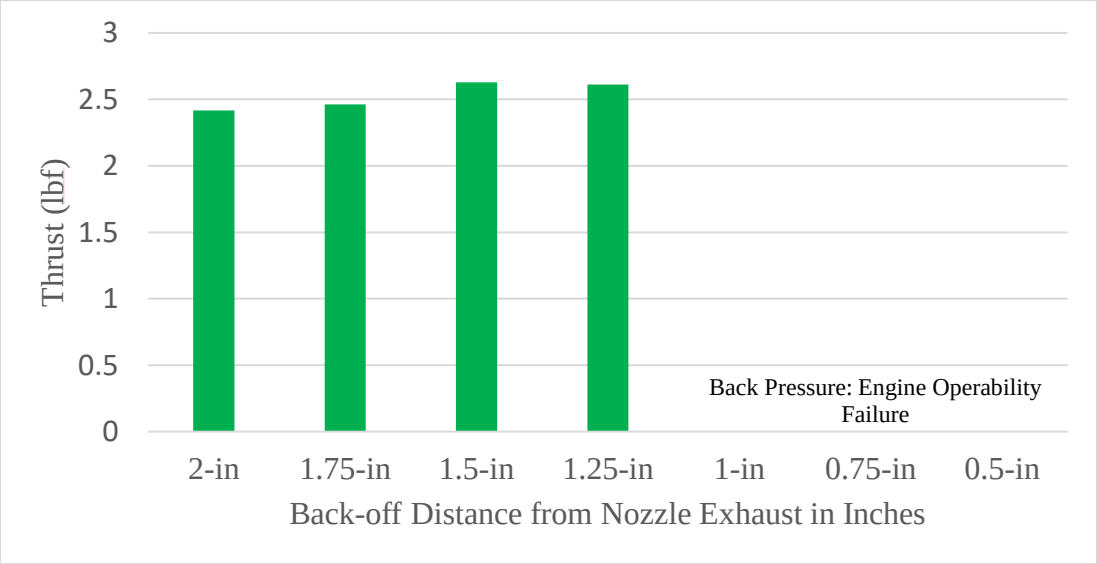

Figure 42: Jet Thrust vs Backoff Distance for 0.945-in exit nozzle diameter

Over the allotted time the nozzles were left at their distances thrust was recorded and the average thrust recorded at these distances was then calculated. The average thrust at each distance is what is represented at each of the figures above. A maximum thrust of 2.8lbf recorded with the 1.102-in nozzle occurred when the nozzle was closest to the exhaust pipes as seen in Figure 40. Referencing figures 38 and 39, an overall negative impact can be seen with the 1.575-in and 1.417-in nozzles. Although the impact isn't significant, it is not positive. Referencing figures 40,

41, and 42; there is an interesting distinction at the 1.25-in backoff distance and the 0.5-in backoff distance. All three of these graphs seem to show a peak at the 1.25-in. Looking specifically at figures 40 and 41 now, another peak is shown at the 0.5-in backoff distance. If the 0.945-in nozzle did not show certain operability errors is possible that the same trend at the 0.5-in distance could have been seen. The maximum thrust record with the 1.260-in was 2.7lbf. The maximum thrust recorded with the 1.575-in nozzle was 2.78lbf and this occurred somewhere in between the seven observation points. At 2 inches off the exhaust pipe the 1.102 nozzle has providing 2.5lbf of jet thrust and at 0.5 inches there is a peak thrust of 2.77lbf, this is a 10.8% increase in thrust. Because of this trend with a smaller nozzle diameter, 0.945-in, was fixed to the exhaust pipes, this will be discussed later. However, looking at Figure 38 the maximum thrust occurred when the nozzles were farther away from the exhaust pipes. Moving the 1.575-in nozzles closer to the exhaust pipes has a very negative impact on the jet thrust. The peak thrust of 2.78lbf and the thrust recorded at 0.5 inches from the exhaust pipe was 1.88lbf, this is a 32% decrease in jet thrust. Based on this testing it can be concluded that the smaller nozzle overall performed better than the larger nozzle. The small nozzle has better performance because the flow area is optimal. The 0.945-in nozzle caused the engine operability to fail before they could be brought as close as possible to the exhaust pipes.

4.2 Variable Nozzle Distance Turboprop Testing

The 1.102-in, 1.260-in, 1.417-in, and 1.575-in nozzle were both in turboprop mode and turbojet mode and tested at distances of 2-in and 0.5-in. The engine was brought up to full throttle and then the nozzle distance was changed while data was being recorded. The figure below shows the results of these tests.

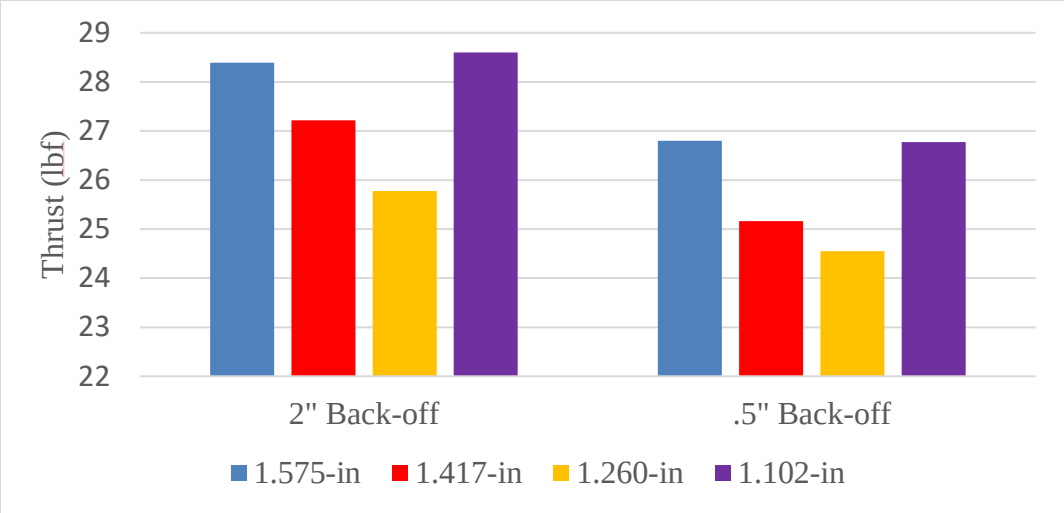

Figure 43: Effect of Exhaust Nozzle Backoff Distance on Turboprop Thrust

Looking at the trends in Figure 43, there is a small negative impact on turboprop thrust when the nozzles is moved closer to the exhaust pipes. With all nozzle configurations a peak thrust anywhere from 25 to 28lbf. Also, in both instances the thrust dips down just below 24 to 27lbf of thrust whenever the nozzles are closest to the exhaust pipes, only loosing 1lb of thrust when the nozzle was closest to the exhaust pipes. However, this is around only a 3.5% to 4% decrease in thrust. Individual graphs for each testing configuration are included in the appendix. Fixing nozzles to the exhaust pipes is further justifiable with this experiment.

4.3 Fixed Nozzle Turbojet and Turboprop Testing

The 0.945-in nozzle was fixed to the exhaust pipes and test in both turboprop mode and turbojet mode test. An attempt to bring the engine up to full throttle was done, but the potential mechanical errors restricted the engine from operating properly. The two figures below show the results of these tests.

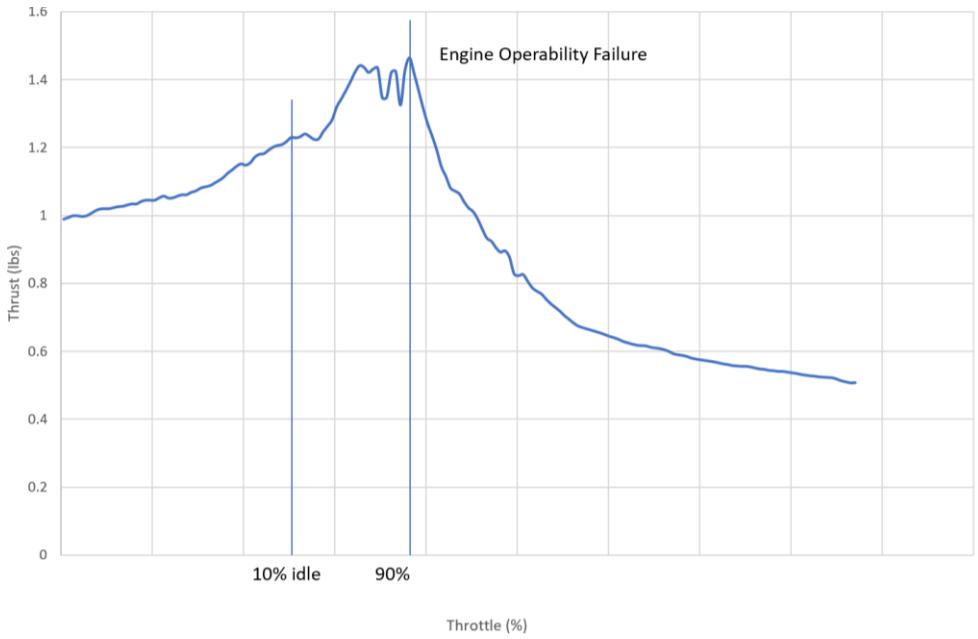

Figure 44: Jet Thrust with Fixed Nozzle vs. Throttle (0.945-in)

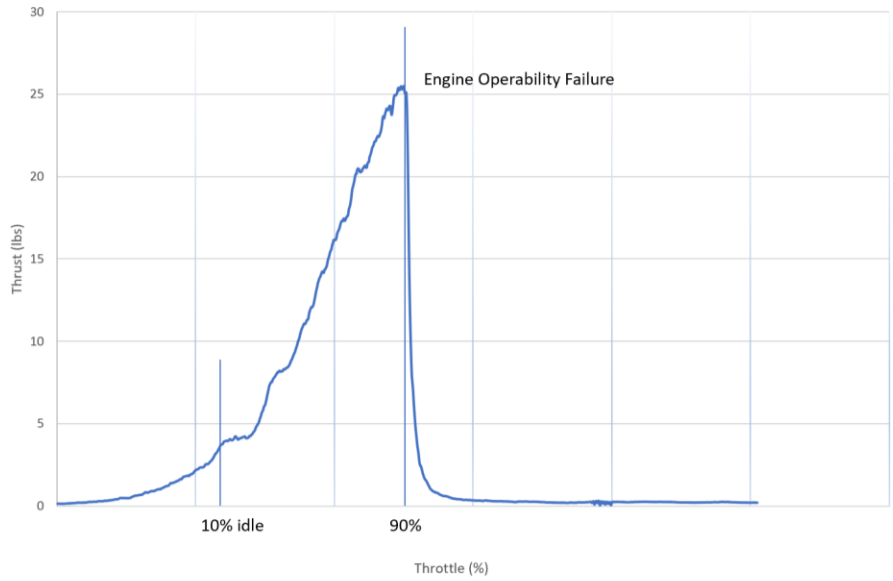

Figure 45: Propeller Thrust with Fixed Nozzle vs. Throttle (0.945-in)

While the result for both configurations with the fixed nozzle is very promising, there is one issue that arises. It is believed that there is some back pressure within the engine prohibiting it

from running properly and causing the engine to fail. While running the engine in turbojet mode a max thrust of 1.46lbf was recorded, and this occurred at only 20% of the engine throttle. The engine was on track to reach the previously recoded max turboprop thrust of 28lbf however, at 90% throttle the engine failed. Only assumptions can be made as to why the engine is unable to run in this fixed nozzle configuration, but if it can be managed then the results should prove to be very promising.

4.4 Uncertainty Analysis

Sources of error for thrust data can come from the load cell itself. Looking back at Table 3, the load cell has a read-out error of 0.02%. The following equation is what was used to find the uncertainty factor in the data itself.

$$U = \sqrt{\beta^2 + P^2} \tag{33}$$

U is the uncertainty factor, β is the uncertainty bias, and P is the precision error. The uncertainty bias is found by using the read-out error given by the load cell company and multiplying by the average thrust recorded over a certain time, or in this case during specific backoff distance. The precision error is found dividing the average thrust recorded at a specific backoff distance by the standard deviation of that same backoff distance. The table below represents all nozzle diameters at each backoff distance and each configuration's average, uncertainty bias, precision error, and uncertainty factor.

Table 7: Uncertainty Analysis on Nozzle Geometries vs. Backoff Distances

1.575-in Nozzle				
	Average Thrust (lbf)	β (%)	P (%)	U (%)
2-in	2.818	0.056	1.29	1.29
1.75-in	2.769	0.055	4.87	4.88
1.5-in	2.616	0.052	1.46	1.47
1.25-in	2.604	0.052	1.44	1.44
1-in	2.65	0.053	1.09	1.09
0.75-in	2.669	0.053	.95	.96
0.5-in	2.711	0.043	17.9	17.9
1.417-in Nozzle				
Backoff Distance	Average Thrust (lbf)	β (%)	P (%)	U (%)
2-in	2.689	0.054	1.18	1.18
1.75-in	2.739	0.055	3.14	3.14
1.5-in	2.553	0.051	4.15	4.15
1.25-in	2.531	0.051	1.77	1.78
1-in	2.462	0.049	2.08	2.08
0.75-in	2.357	0.047	2.43	2.44
0.5-in	2.131	0.045	10.7	10.7

1.260-in Nozzle				
Backoff Distance	Average Thrust (lbf)	β (%)	P (%)	U (%)
2-in	1.978	0.040	1.78	1.79
1.75-in	1.994	0.040	1.40	1.40
1.5-in	2.13	0.043	2.62	2.62
1.25-in	2.187	0.044	2.42	2.43
1-in	2.15	0.043	5.34	5.35
0.75-in	2.14	0.043	2.72	2.73
0.5-in	2.156	0.043	2.44	2.44
1.102-in Nozzle				
Backoff Distance	Average Thrust (lbf)	β (%)	P (%)	U (%)
2-in	2.563	0.051	2.40	2.41
1.75-in	2.602	0.052	.972	.973
1.5-in	2.679	0.054	3.32	3.32
1.25-in	2.729	0.055	2.62	2.63
1-in	2.705	0.054	1.94	1.95
0.75-in	2.745	0.055	1.78	2.72
0.5-in	2.8	0.056	4.03	4.04

0.945-in Nozzle				
Backoff Distance	Average Thrust (lbf)	β (%)	P (%)	U (%)
2”	2.416	0.048	2.54	2.54
1.75”	2.462	0.049	2.35	2.36
1.5-in	2.628	0.043	1.46	1.47
1.25-in	2.612	0.055	1.67	1.68
1-in	0	0	0	0
0.75-in	0	0	0	0
0.5-in	0	0	0	0

For the most part all the uncertainty factors are below 5%. There are a couple of instances, referring to Table 6, where the percentage is greater than 5%. For both the 1.575-in and the 1.417-in nozzle, at the 0.5-in backoff distance, an uncertainty factor of 17% and 10% are calculated. I believe the reason for this high of a percentage is due to the sudden drop in thrust performance in these configurations.

4.5 Fixed vs. Folding Propeller Results

Figure 46 depicts performance of fixed 2-blade 20x10 APC and folding 2-blade 20x10 propellers. On the left-hand side, the scale for thrust coefficient is represented. On the right side of the figure propeller efficiency is represented. Both are in correlation with advanced ratio. The C_T results in Figure 46 are extremely similar. The decrease of C_T observed can be attributed to the lower Reynolds number. Lower Reynolds number typically have lower efficiencies because it is harder for the flow to stay attached to the propeller. The η_p results in both Figure 46 remain similar between fixed and folding variants. Given that there is no significant difference in the performance of a fixed blade propeller in contrast to a folding blade propeller, a folding blade propeller would be suitable for RATO launch applications.

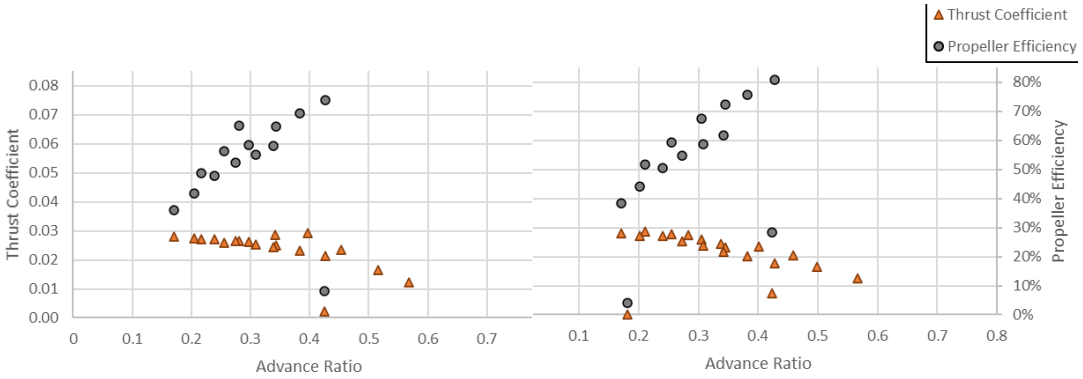

Figure 46: Comparison of C_t and η_p Fixed (left) and Folding (right) 2-Blade, 20x10 Propellers

CHAPTER V

CONCLUSION

5.1 Summary

The results of this study present the testing of a variety of different nozzles at varying distances for both turbojet and turboprop mode. Running the engine in turbojet mode had quite a few issues. First, the engine was meant to operate as a turboprop. Restricting the engine's ability to run as a turboprop presented issues during the startup cycle. The engine at times would not meet the required temperatures to continue to the next stage of the startup sequence, often because the engine got too hot. Second, if the engine managed to complete the startup sequence and officially begin running, bringing the nozzles closer to the engine would at times create an excess of back pressure within the engine. The back pressure would often prohibit the engine's ability to meet the RPM being demanded by the throttle control. In most instances the engine's inability to maintain the RPM caused by the back pressure would cause the engine to ultimately stop running completely and start the cool down cycle. Aside from the engine's inconsistency in reliability during the turbojet testing, adequate thrust could not be produced. The max thrust ever produced in any nozzle configuration at any distance was close to three pounds. There was only one good observation from testing the engine in turbojet mode. With some nozzle geometries, a positive thrust trend could be seen whenever the nozzles were brought closer to the exhaust pipes. The

engine is not capable of producing adequate jet thrust to maintain cruise or high-speed pursuit. However, the turboprop results prove to be more promising. Testing the engine in turboprop mode proved to show more positive results. There was only one instance where the engine operability was prohibited. That was during the fixed nozzle test. The testing done in turboprop mode showed that there is a negligible impact on the nozzle distance relative to propeller thrust.

5.2 Recommendations

While the engine cannot produce adequate turbojet thrust for the purposed mission, it does still produce some thrust that could be useful for something. A RATO launch with a folding propeller mounted to the engine is still a very attainable concept. The folding propeller would initially start out in the locked configuration before and during the RATO launch itself. Then after the aircraft is at altitude and speed, the lock would be released allowing the propeller to spin freely enabling the aircraft to cruise and loiter respectively. The significance of producing a small amount of turbojet thrust could allow for a smooth transition from the RATO launch to turboprop methods of power. In addition to this project, a mechanism capable of keeping the folding propeller locked and releasing the folding propeller needs to be developed. The locking mechanism was crucial to the initial concept of a dual-mode engine and is still very crucial to the concept of RATO launching a small aircraft. Methods using a linear actuator or potentially a clutch system are still in the early developmental stages regarding a locking mechanism. For future projects, I would recommend the development of a propeller locking mechanism and RATO launch with a folding propeller be investigated.

REFERENCES

1. Aviation, GE. n.d. "www.geaviation.com/military/engines/ge-adaptive-cycle-engine." *www.geaviation.com.* https://www.geaviation.com/military/engines/ge-adaptive-cycle-engine.
2. Cat, Jet. 21016. "Jet Cat Data Sheet." *Jet Cat.* April 2. https://www.chiefaircraft.com/pdf/jetcat-data.pdf.
3. Durkee, Matt. 2018. "Turbojet Ejector and Propeller Aft Assembly for Small Unmanned Aircraft ." *56th AIAA Aerospace Sciences Meeting & Exhibit.*
4. n.d. *futek.com.* https://www.futek.com/store/load-cells/oem-load-cells/oem-LSM300.
5. Jack D. Mattingly, Keith M. Boyer. 2016. *Elements of Propulsion: Gas Turbines and .* Blacksburg: AIAA.
6. KingTech. 2016. *KingTech Turbines Engine Manual.*
7. Matt Durkee, Dr. Kurt Rouser. 2019. *TURBOPROP PERFORMANCE AND ACOUSTIC .* Stillwater: Oklahoma State University.
8. Oglesby, Britt A. 2014. *EXPERIMENTAL STUDY OF A SMALL TURBOJET FOR USE IN AN UNMANNED AIRCRAFT SYSTEM.* Master's Thesis, Stillwater: Oklahoma State University.
9. Real, KC. 2019. "Investigation of a Geared Turbofan for Small Unmanned Aircraft Systems." *57th AIAA Aerospace Sciences Meeting & Exhibit.* AIAA.
10. Welliver, E. A. Willis and A. D. n.d. "SUPERSONIC VARIABLE-CYCLE ENGINES." *American Institute of Aeronautics and Astronautics and the Society of Automotive Engineers.*
11. Willis, Edward. n.d. "VARIABLE-CYCLE ENGINES FOR SUPERSONIC CRUISE." *AGARD Propulsion Conference.*
12. n.d. *www.hampsonlife.com.* http://www.hampsonlife.com/conecalculator.php.

13. Brand J. and Selig, M. 2011. "Propeller Performance Data at Low Reynolds Numbers." Champaign-Urbana: University of Illinois.

14. R.W. Deters, G.K. Ananda Krishnan, and M.S. Selig. 2014. "Reynolds Number Effects on Small Scale Propellers." *32nd AIAA applied aerodynamic conference.* Champaign-Urbana: University of Illinois. 2151.

15. J.W., McCrink M.H. and Gregory. 2015. "Blade Element Momentum Modeling of Low-Re Small UAS Electric Propulsion Systems." Columbus: Ohio State University.

16. Engineering, Department of Aeronautical. n.d. "Propeller Theory."

APPENDICES

$\pi_c := 2.1$

$Tt4 := 1400\,°F = 1859.7\,R$

$\pi_b := .92 \quad \eta_b := .94$

$\pi_n := .98 \quad \pi_{d.max} := .96 \quad e_c := .88 \quad e_t := .89 \quad \eta_{mech} := .99 \quad V := 150mph$

$\gamma_c := 1.4 \quad \gamma_t := 1.36 \quad c_{cp} := .24\frac{BTU}{lbm \cdot R} \quad c_{pt} := .275\frac{BTU}{lbm \cdot R} \quad h_{PR} := 18400\frac{BTU}{lbm}$

Atmospheric conditions: 2000 ft

$a_0 := 756mph \qquad g_c := 32.2\frac{lbm \cdot ft}{lbf \cdot s^2} \qquad M_0 := \frac{V}{a_0} = 0.198$

$p_0 := 13.66psi$

$P0\_P9 := 1$

$T_0 := 51.9\,°F = 511.57\,R$

Bundle

$Tt0\_T0 := 1 + \frac{\gamma_c - 1}{2} \cdot M_0 = 1.04 \qquad \tau_r := Tt0\_T0 = 1.04$

$Tt0 := T_0 \cdot \tau_r = 531.87\,R$

$Pt0\_P0 := \tau_r^{\frac{\gamma}{\gamma - 1}} = 0.948 \qquad \pi_r := Pt0\_P0 = 0.948$

$Pt0 := p_0 = 13.66\,psi$

$Pt2 := Pt0 = 13.66\,psi$

$V_0 := M_0 \cdot a_0 = 220\,\frac{ft}{s}$

Inlet

$\eta_r := 1$

$\pi_d := \pi_{d.max} \cdot \eta_r = 0.96$

Compressor

$Tt2 := Tt0 = 531.87 \cdot R$

$\tau_c := \pi_c^{\frac{\gamma_c - 1}{\gamma_c \cdot e_c}} = 1.272$

$Pt3 := \pi_c \cdot Pt2 = 28.686 \cdot psi$ $\quad$ $Pt4 := \pi_b \cdot Pt3 = 26.391 \cdot psi$

$Tt3 := \tau_c \cdot Tt2 = 676.741 \cdot R$

Burner $\quad$ $mdot := .3 \frac{lbm}{s}$

$$f := \frac{c_{pt} \cdot Tt4 - c_{cp} \cdot Tt3}{h_{PR} \cdot \eta_b - c_{pt} \cdot Tt4} = 0.021$$

$$mdot_f := f \cdot mdot = 0.0028294 \frac{kg}{s}$$

Turbine

$$Tt5 := Tt4 - \frac{c_{cp} \cdot (Tt3 - Tt2)}{(1 + f) \cdot \eta_{mech} \cdot c_{pt}} = 1734.562 \cdot R$$

$$\tau_t := \frac{Tt5}{Tt4} = 0.933$$

$$\pi_t := \tau_t^{\frac{\gamma_t}{(\gamma_t - 1) \cdot e_t}} = 0.744$$

$Pt5 := \pi_t \cdot Pt4 = 19.637 \cdot psi$

Nozzle

$$Pt9\_P9 := \pi_r \cdot \pi_d \cdot \pi_c \cdot \pi_b \cdot \pi_t \cdot \pi_n \cdot P0\_P9 = 1.282$$

$$Tt9\_T9 := Pt9\_P9^{\frac{\gamma_t - 1}{\gamma_t}} = 1.068$$

$$Tt9 := Tt5 = 1734.6 \cdot R$$

$$T9 := \frac{Tt9}{Tt9\_T9} = 1624.014 \cdot R$$

$$V_9 := \sqrt{(Tt9 - T9) \cdot 2 \cdot g_c \cdot c_{pt}} = 1234.303 \cdot \frac{ft}{s}$$

Figures Of Merit

$$F\_mdot_0 := \frac{(1 + f) \cdot V_9 - V_0}{g_c} = 32.297 \cdot \frac{lbf}{\frac{lbm}{s}}$$

$$Thrust := F\_mdot_0 \cdot mdot = 9.689 \cdot lbf$$

$$SFC := \frac{f \cdot g}{F\_mdot_0} = 2.318 \cdot \frac{1}{hr}$$

$$\eta_{th} := \frac{(1 + f) \cdot V_9^2 - V_0^2}{2 \cdot g_c \cdot f \cdot h_{PR}} = 0.079$$

$$\eta_p := \frac{2 \cdot g_c \cdot V_0 \cdot F\_mdot_0}{(1 + f) \cdot V_9^2 - V_0^2} = 0.304$$

$$\eta_0 := \eta_{th} \cdot \eta_p = 0.024$$

Turboprop

$F_{prop} := 28lbf \qquad W_{prop} := 5.2kW = 5.2 \cdot kW$

$F_C := 10lbf$

$V_{prop} := .05 \cdot a_0 = 55.44 \cdot \frac{ft}{s}$

$\eta_{prop} := \frac{F_{prop} \cdot V_{prop}}{W_{prop}} = 0.405$

$C_C := (1 - \gamma) \cdot M_0 \cdot \left(\frac{V_9}{a_0} - M_0 \right) = 0.077$

$C_{prop} := \frac{\eta_{prop} \cdot W_{prop}}{mdot \cdot c_{cp} \cdot T_0} = 0.054$

$C_{tot} := C_{prop} + C_C = 0.131$

Figures of Merit for Turborprop

$W\_mdot := C_{tot} \cdot c_{cp} \cdot T_0 = 16.956 \cdot \frac{kW}{\frac{lbm}{s}}$

$F\_mdot_{prop} := \frac{C_{tot} \cdot c_{cp} \cdot T_0}{V_0} = 56.845 \cdot \frac{lbf}{\frac{lbm}{s}}$

$SFC_{prop} := \frac{f}{F\_mdot_{prop}} = 1.317 \cdot \frac{lbm}{lbf \cdot hr}$

GIVEN

Aircraft Data:

$W_e := 12lbf$ $nE := 1$ $b := 9ft$

$W_f := 6lbf$ $M_{ref} := .2$ $c := 4in$

$S_{wing} := b \cdot c = 3\,ft^2$

Estimated Drag Polar:

$K_1 := \frac{1}{\pi \cdot .9 \cdot 2} = 0.177$ $C_{D0} := .013$

Mission Data:

$W_{factor\_4} := 1.02$ $Alf_{cruise} := 2000ft$

$M_{cruise} := M_{ref}$ $M_{loiter} := .05$

$R_{cruise} := 50mi$

Atmospheric Data:

$P_{alt} := 13.66 \frac{lbf}{in^2}$ $\rho_{alt} := .0749 \frac{lbm}{ft^3}$

$T_{alt} := 52F$ $a_{alt} := 756.06mph$

Installation Loss Model:

$\Phi_{cruise} := .05$ $\Phi_{loiter} := .05$

Initial Dash Starting Weight:

$W_1 := W_e + W_f = 18 \cdot lbf$

Return Cruise Ending Weight:

$W_4 := W_{factor\_4} \cdot W_e = 12.24 \cdot lbf$

Dash Velocity:

$$V_{cruise} := M_{cruise} \cdot a_{alt} = 221.778 \cdot \frac{ft}{s}$$

Initial Cruise Lift Coefficient:

$$C_{L1} := \frac{2 \cdot W_1}{\rho_{alt} \cdot V_{cruise}^{2} \cdot S_{wing}} = 0.105$$

Initial Cruise Drag Coefficient:

$$C_{D1} := C_{D0} + K_1 \cdot C_{L1}^{2} = 0.015$$

Initial Cruise Uninstalled Thrust Required:

$$F_{min\_3} := \frac{\frac{1}{2} \cdot \rho_{alt} \cdot V_{cruise}^{2} \cdot C_{D1} \cdot S_{wing}}{\left(1 - \Phi_{cruise}\right) \cdot nE} = 2.701 \cdot lbf$$

Initial Cruise Uninstalled Thrust Required:

$$SFC_{ref} := 2.29 \frac{lbm}{hr \cdot lbf} \quad g_c := 32.2 \frac{lbm \cdot ft}{lbf \cdot s^{2}}$$

$$SFC_{1\_2} := SFC_{ref} = 2.29 \cdot \frac{lbm}{hr \cdot lbf}$$

Initial Cruise Ending Weight:

$$W_2 := \left(\sqrt{W_1} - \sqrt{\frac{\rho_{alt} \cdot S_{wing}}{2 \cdot C_{L1}}} \cdot \frac{\frac{R_{cruise}}{2} \cdot SFC_{1\_2} \cdot g}{1 - \Phi_{cruise}} \cdot C_{D1} \right)^{2} = 16.013 \cdot lbf$$

Return Cruise Lift Coefficient:

$$C_{L4} := \frac{2 \cdot W_4}{\rho_{alt} \cdot V_{cruise}^{2} \cdot S_{wing}} = 0.071$$

$$C_{D4} := C_{D0} + K_1 \cdot C_{L4}^{2} = 0.014$$

Return Cruise Uninstalled SFC:

$$SFC_{3\_4} := 1 \frac{lbm}{hr \cdot lbf}$$

Note : Turboprop partial throttle estimate, KC et al.

Return Cruise Starting Weight:

$$W_3 := \left[\sqrt{W_4} + \sqrt{\frac{\rho_{alt} \cdot S_{wing}}{2 \cdot C_{L4}}} \cdot \frac{R_{cruise} \cdot SFC_{3\_4} \cdot g \cdot C_{D4}}{2 \cdot \left(1 - \Phi_{cruise}\right)} \right]^2 = 13.085 \cdot lbf$$

Return Cruise Lift Coefficient:

$$C_{L3} := \frac{2 \cdot W_3}{\rho_{alt} \cdot V_{cruise}^{2} \cdot S_{wing}} = 0.076$$

Return Cruise Drag Coefficient:

$$C_{D3} := C_{D0} + K_1 \cdot C_{L3}^{2} = 0.014$$

Return Cruise Uninstalled Thrust Required:

$$F_{min\_3} := \frac{\frac{1}{2} \cdot \rho_{alt} \cdot V_{cruise}^{2} \cdot C_{D3} \cdot S_{wing}}{\left(1 - \Phi_{cruise}\right) \cdot nE} = 2.536 \cdot lbf$$

Fuel available for loiter:

$$W_{fuel\_loiter} := W_2 - W_3 = 2.928 \cdot lbf$$

Loiter velocity:

$$V_{loiter} := M_{loiter} \cdot a_{alt} = 55.444 \cdot \frac{ft}{s}$$

Loiter Initial Lift Coefficient:

$$C_{L2} := \frac{2 \cdot W_2}{\rho_{alt} \cdot V_{loiter}^{\ 2} \cdot S_{wing}} = 1.492$$

$$C_{D2} := 2 \cdot K_1 \cdot C_{L2}^{\ 2} = 0.787$$

Loiter Uninstalled Thrust Required:

$$F_{min\_2} := \frac{\frac{1}{2} \cdot \rho_{alt} \cdot V_{loiter}^{\ 2} \cdot S_{wing} \cdot C_{D2}}{\left(1 - \Phi_{loiter}\right) \cdot nE} = 8.892 \cdot lbf$$

Loiter Maximum Endurance:

$$E_{loiter} := \frac{1}{g} \frac{\left(1 - \Phi_{loiter}\right)}{SFC_{3\_4}} \cdot \frac{C_{L2}}{C_{D2}} \cdot \ln\left(\frac{W_2}{W_3}\right) = 21.815 \cdot min$$

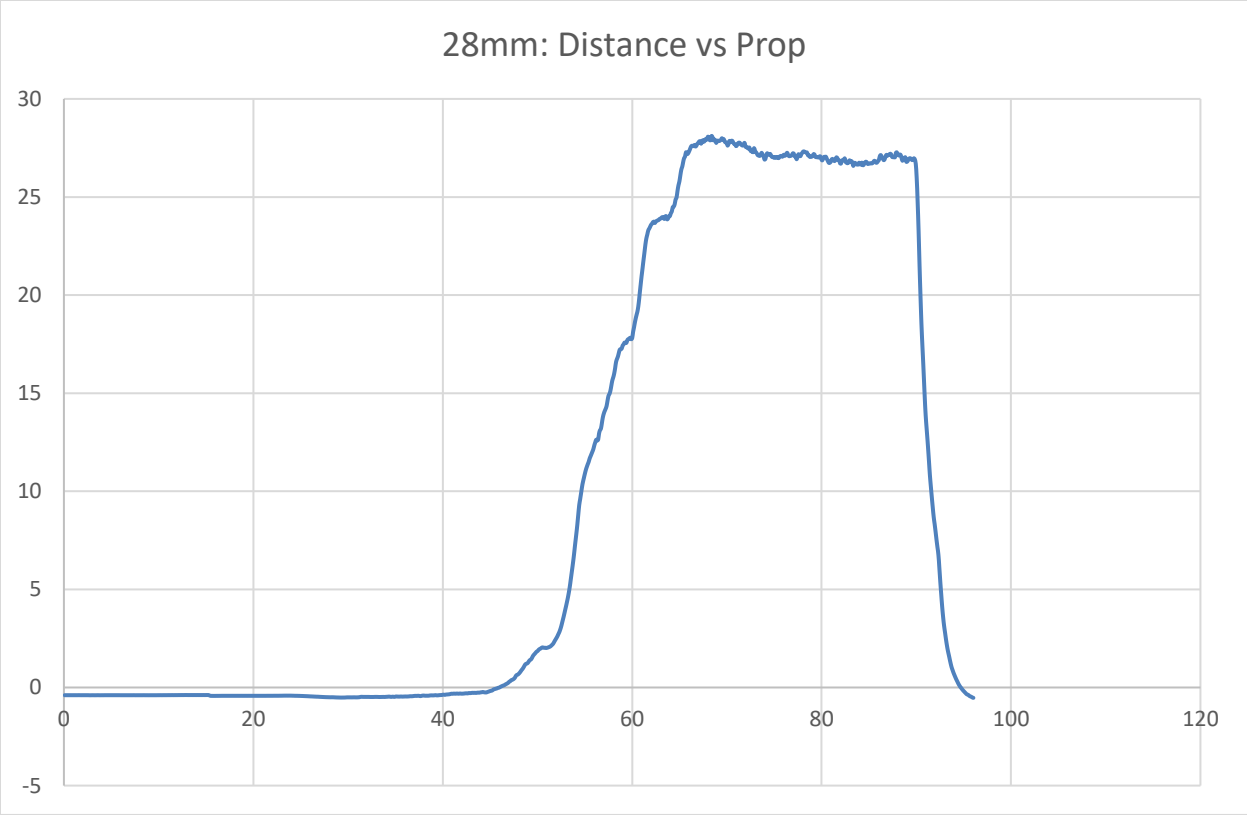
28mm: Distance vs Prop
30
25
20
15
10
5
0
-5
0
20
40
60
80
100
120

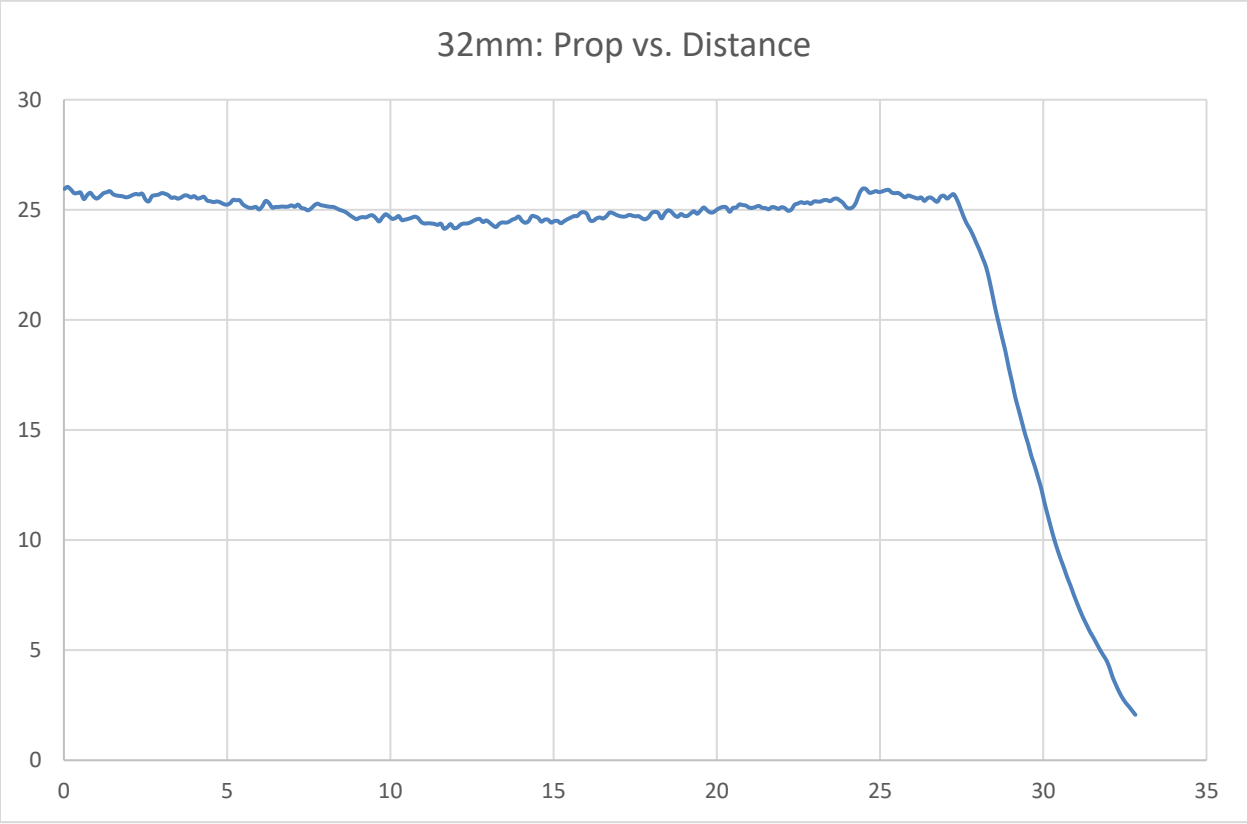
32mm: Prop vs. Distance
30
25
20
15
10
5
0
0
5
10
15
20
25
30
35

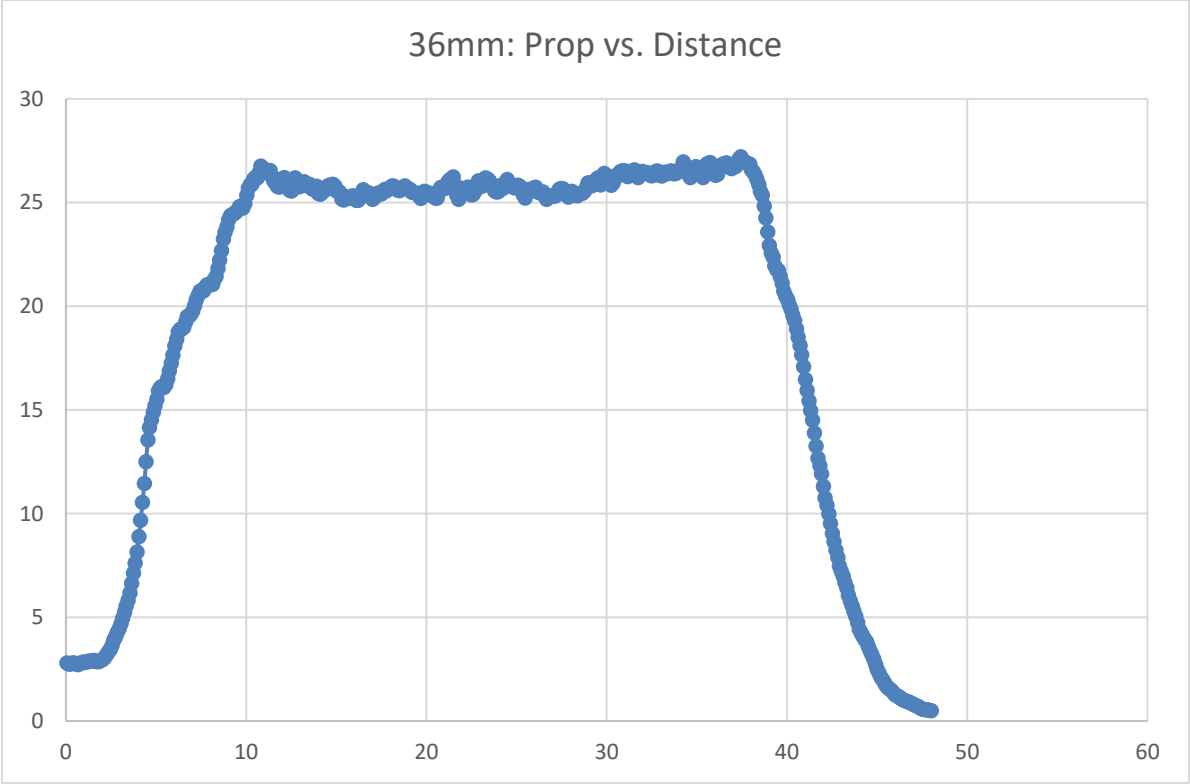
36mm: Prop vs. Distance
30
25
20
15
10
5
0
0
10
20
30
40
50
60

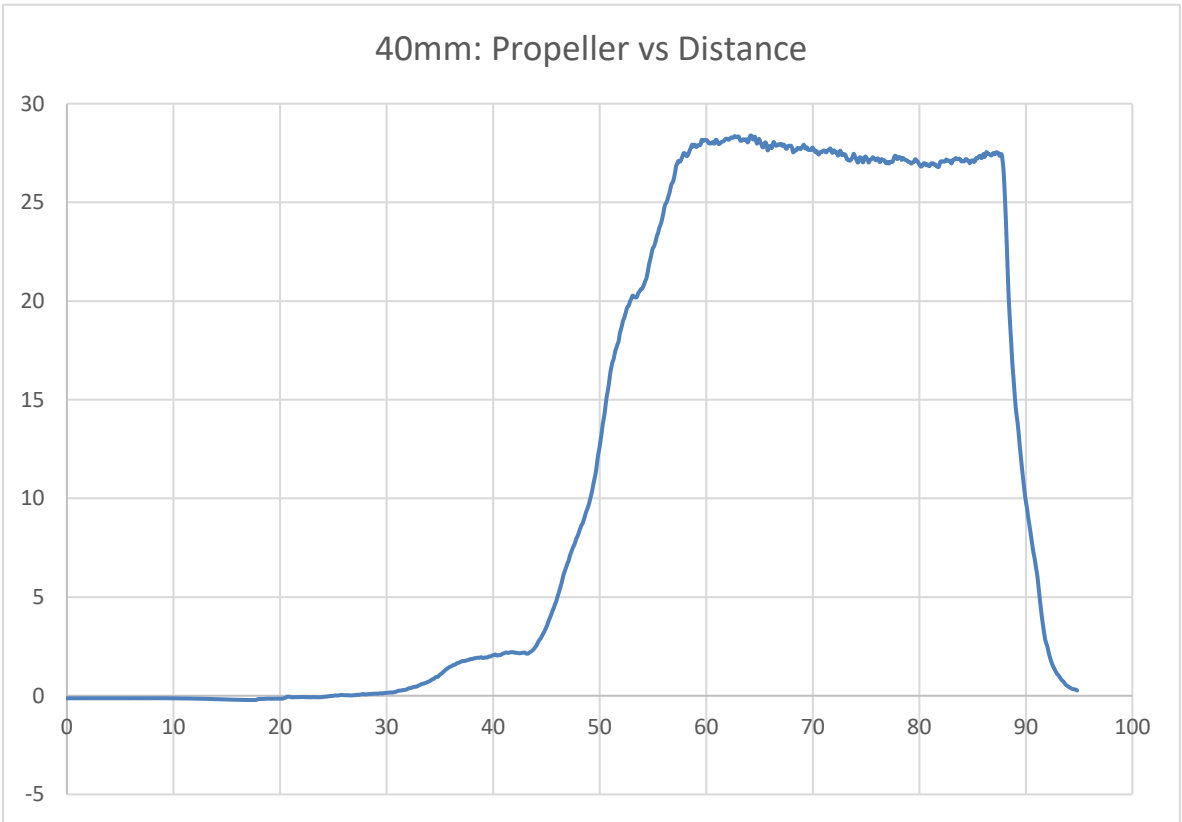
40mm: Propeller vs Distance
30
25
20
15
10
5
0
-5
0
10
20
30
40
50
60
70
80
90
100

VITA

Trey Morgan Schinzler

Candidate for the Degree of

Master of Science

Thesis: EVALUATION OF A DUAL-MODE, TURBOJET/TURBOPROP ENGINE FOR UNMANNED AIRCRAFT

Major Field: Mechanical and Aerospace Engineering

Biographical:

Education:

Completed the requirements for the Master of Science in Mechanical and Aerospace Engineering at Oklahoma State University, Stillwater, Oklahoma in May, 2022.

Completed the requirements for the Bachelor of Science in Aerospace Engineering at Oklahoma State University, Stillwater, Oklahoma in 2020.

Completed the requirements for the Bachelor of Science in Mechanical Engineering at Oklahoma State University, Stillwater, Oklahoma in 2020.

Experience:

Graduate Research Assistant – Oklahoma State University, Stillwater, OK
Graduate Teaching Assistant – Oklahoma State University, Stillwater, OK

Professional Memberships:

AIAA, SAE